DEVELOPMENT OF A 6 DOF COMPLIANT PARALLEL MECHANISM TO SENSE AND CONTROL THE FORCE-TORQUE AND DISPLACEMENT OF A SERIAL ROBOT MANIPULATOR

By

SUBRAT NAYAK

A THESIS PRESENTED TO THE GRADUATE SCHOOL
OF THE UNIVERSITY OF FLORIDA IN PARTIAL FULFILLMENT
OF THE REQUIREMENTS FOR THE DEGREE OF
MASTER OF SCIENCE

UNIVERSITY OF FLORIDA

2009

This thesis is dedicated to my mother, Sulochana Nayak and my father, Sunakar Nayak

ACKNOWLEDGMENTS

I would like to express my thanks to Dr. A. Antonio Arroyo for being my Committee Chair, motivating me to do research in robotics, sharing his technical expertise and providing me the necessary workspace and equipment at the Machine Intelligence Lab (MIL).

I am grateful to Dr. Carl D. Crane III for being my Committee Co-Chair. I am grateful to him for suggesting the topic for my thesis, in-depth teaching in Geometry of Robots, providing his technical expertise and necessary workspace and equipment at the Centre for Intelligent Machines and Robotics (CIMAR).

I would like to express my thanks to Dr. Herman Lam for his time and willingness to serve on my committee.

I am indebted to Dr. Eric M. Schwartz for his continuous support and encouragement in everything that I worked on during my time as a master's student. He also served as a extra special member in my Supervisory Committee.

I would like to express my gratitude to Jeff Johnson and Jose Morales in MIL and Shannon Ridgeway and Moses Anubi in CIMAR for helping me on various aspects of my thesis. I owe an appreciation to Dr Bo Zhang whose PhD dissertation and mechanical design formed the foundation for my work.

Last but not the least, I wish to thank my father Sunakar and mother Sulochana for trusting me on whatever I wished to do. I also thank my girl friend and fiancée, Aditi for her patience and support. I also wish to thank my brother, Sameer and my sister, Snigdha for their moral support.

TABLE OF CONTENTS

LIST OF TABLES

LIST OF FIGURES

LIST OF ABBREVIATIONS

AC / DC	Alternating Current and Direct Current
ASCII	American Standard Code of Information Interchange
ASIC	Application Specific Integrated circuits are customized for a particular use, rather than intended for general-purpose use
CTS	Clear To Send is a RS232 Signal line. It is asserted by DCE to acknowledge RTS and allow DTE to transmit.
DLL	Dynamic Link Library
DOF	Degrees of Freedom are the set of independent displacements and/or rotations that specify completely the displaced position and orientation of the body or system. A particle that moves in three dimensional space has three translational displacement components as DOFs, while a rigid body would have at most six DOFs including three rotations. Translation is the ability to move without rotating, while rotation is angular motion about some axis.
DSR	Data Set Ready Signal Line is a RS232 Signal line. It is asserted by DCE to indicate the DCE is powered on and is ready to receive commands or data for transmission from the DTE.
DTR	Data Terminal Ready is a RS232 Signal line. It is asserted by DTE to indicate that it is ready to be connected. When this signal is de-asserted, the modem may return to its standby mode, immediately hanging up any calls in progress.
EEPROM	Electrically Erasable Programmable Read Only Memory
FPGA	Field programmable Gate Array
FTDI	Future Technology Devices International Ltd.
LED	Light Emitting Diode
LVDT	Linear Variable Displacement Transducer
PKM	Parallel Kinematic Mechanism or simply a Parallel Platform
RCC	Remote Center Compliance
RS232	Recommended Standard 232 is a standard for serial binary data signals connecting between a DTE (Data Terminal Equipment) and a DCE (Data Circuit-terminating Equipment). It is commonly used in computer serial ports.

RTR	Ready To Receive is a RS232 Signal line. It is asserted (set to logic 0, positive voltage) by DTE to indicate to DCE that DTE is ready to receive data. If in use, this signal appears on the pin that would otherwise be used for Request To Send, and the DCE assumes that RTS is always asserted.
RTS	Request To Send Signal is a RS232 Signal line. It is asserted (set to logic 0, positive voltage) by DTE to prepare DCE to receive data. This may require action on the part of the DCE, e.g. transmitting a carrier or reversing the direction of a half-duplex channel.
SPH	This means Spherical-Prismatic-Hooke. It used to a serial chain of four links connected by a spherical joint, followed by a prismatic joint and then followed by a Hooke joint.
TTL	Transistor Transistor Logic
USB	Universal Serial Bus
USART	Universal Synchronous and Asynchronous Receiver and Transmitter
VCP	Virtual Com Port
VHDL	VHSIC hardware description language, where VHSIC stands for very-high-speed integrated circuit.

Abstract of Thesis Presented to the Graduate School
of the University of Florida in Partial Fulfillment of the
Requirements for the Degree of Master of Sciences

DEVELOPMENT OF A 6 DOF COMPLIANT PARALLEL MECHANISM TO SENSE AND CONTROL THE FORCE-TORQUE AND DISPLACEMENT OF A SERIAL ROBOT MANIPULATOR

By

Subrat Nayak

December 2009

Chair: A. Antonio Arroyo
Co-Chair: Carl D. Crane III
Major: Electrical and Computer Engineering

Parallel mechanisms have been studied for several decades. They have various advantages such as high stiffness, high accuracy and high payload capacity compared to the commonly used serial robots. This thesis focuses on the design of a passive six degree of freedom parallel mechanism that will be installed on the distal end of an industrial serial manipulator i.e. between the tool mounting plate and the end effector or tool. The mechanism can sense and help in simultaneously controlling force-torque and displacement of the serial robot manipulator. The parallel mechanism is comprised of a top platform and a base platform that are connected by six instrumented non-actuated compliant leg connectors. The position and orientation of the top platform relative to the base as well as the external wrench applied to the top platform is determined by measuring the displacements of the individual leg connectors. The serial robot can then move the base platform in order to achieve the desired contact wrench when the top platform gets in contact with the object being manipulated or other objects in the robots environment.

The mechanical system was fabricated. Each leg connector is spring loaded and equipped with optical absolute encoders. Each leg has been individually calibrated to determine the connector properties i.e. spring constant, free length and the transformation from encoder counts to extension of the spring. These properties are used to find the instantaneous length and forces in each leg. The encoder counts for all six leg connectors are simultaneous collected and sent wirelessly to the computer that houses the robot controller. The entire system has been made very compact, battery powered and wireless to ensure no hindrance and minimum change to the structure of the industrial robot manipulator on which its going to be mounted.

The outcome of this research will advance the contact force/torque and pose regulation for in-contact operations of serial industrial robots.

CHAPTER 1
MOTIVATION AND INTRODUCTION

1.1 Motivation

With the development of robotics and control technologies, many tasks can now be done with higher efficiency than ever before. Robots can perform operations in environments that are too dangerous for humans to work in directly. Considering one of the numerous instances, industrial robot manipulators can perform extremely high precision operations in automatic assembly lines. Traditional industrial robots can be positioned and oriented very accurately and moved along a desired trajectory. Hence, simple operations can be achieved by position control alone. Rigid body links and stiff actuation make them capable of high repeatability in positioning and orienting the end effectors. But any positional misalignment of the manipulator would cause unexpected adverse interaction with other objects in its environment. Hence, complex operations require the robot to ensure that the forces and torques applied to the object being manipulated never exceeds allowable limits.

One solution is to integrate a force control scheme into the manipulator position controller where measured forces are fed back in a closed-loop approach. Load cells that are commercially available are capable of measuring spatial wrench but they are quite stiff and the response of the manipulator may not be fast enough to prevent high contact forces or torques. Hence, some sort of compliance control must be used. For example, the simple process of inserting a peg into a hole requires an ability to reposition and reorient the peg based on sensed contact forces. A traditional solution to this problem is to chamfer the edge of the hole, taper the end of the peg, and/or use a Remote Center Compliance (RCC) device, such as shown in Figure 1-1, between the

end effector tool mounting plate and the peg. Here the RCC has high axial stiffness, but low lateral stiffness which when combined with the chamfer applied to the hole, allows for the peg insertion when there is slight position misalignment.

Each actuator contributes to the net force/torque that is applied to the end effector link causing it to either accelerate or influence the contact force and torque if the motion is restricted by the environment. Since motions are provided serially, the effects of control and actuation errors become compounded.

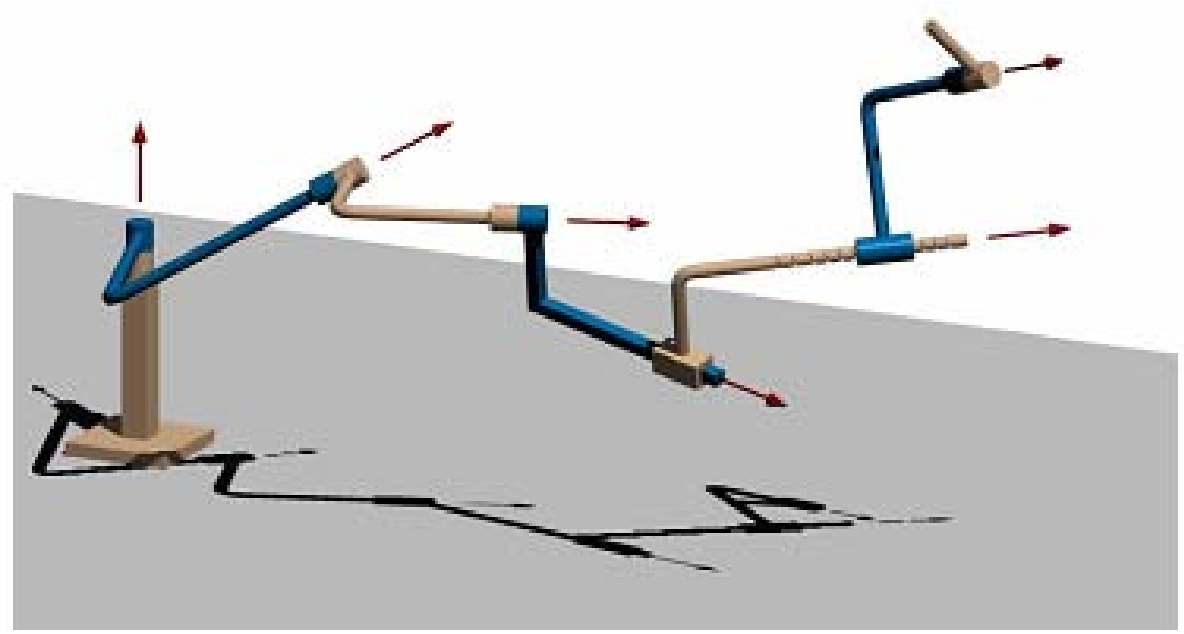

Figure 1-2. Generalized structure of a serial manipulator

Compared to the serial manipulator, the parallel manipulator is a closed-loop mechanism in which the end-effecter (top mobile platform) is connected to the fixed base platform by at least two independent kinematic chains as shown in Figure 1-3. The multiple closed loops improve the stiffness of the manipulator because all the leg connectors sustain the payload in a distributive manner. The problem of end-point positioning error is also reduced due to no accumulation of errors. Hence this type of manipulator enjoys the advantages of compactness, high speed, high accuracy, high loading capacity and high stiffness compared to serial manipulators. Disadvantages, however, include complexity of analysis and limited work space due to connector actuation limits and interference.

The parallel mechanism is a good counterpart and necessary complement to that of the serial manipulator. It is very useful to combine these two types of structures to utilize the advantages of both and reduce their disadvantages.

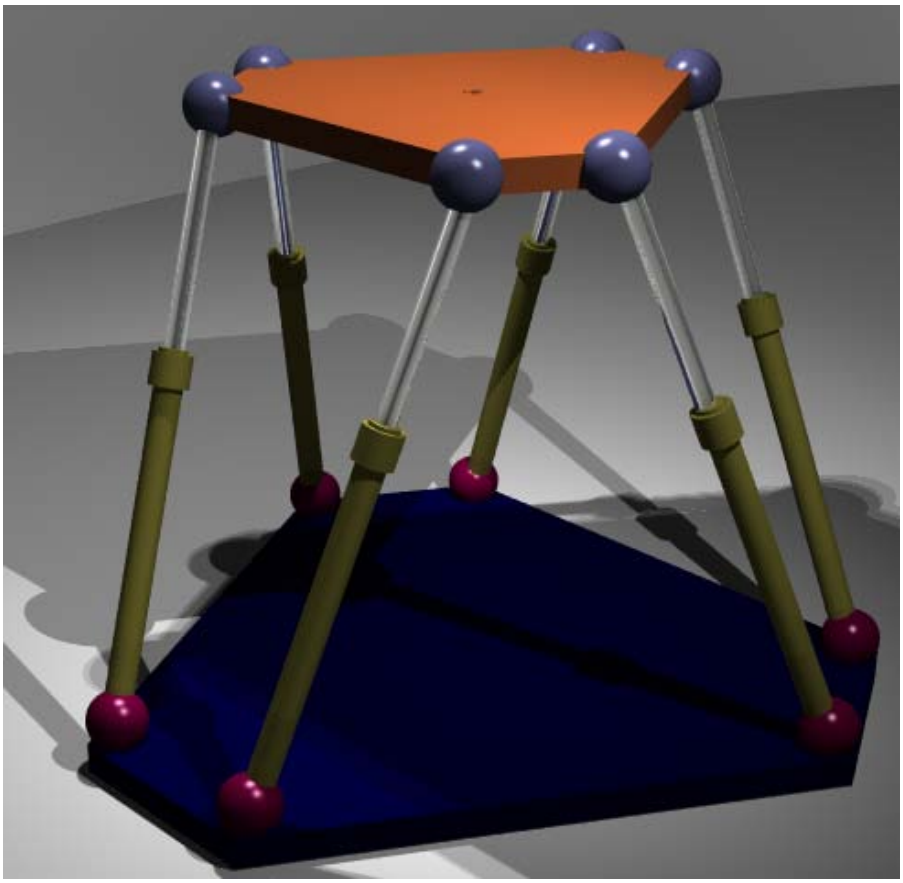

Figure 1-3. Parallel manipulator

One of the complementary applications is force control of serial manipulator by mounting a parallel manipulator at its end. This thesis focuses on the design and development of a parallel manipulator for such an application. A commercially available serial industrial manipulator is being augmented by attaching a compliant in-parallel platform to the end effector plate so that the contact forces can be effectively controlled as shown in Figure 1-4.

The forward analysis of a manipulator is the process of finding the position and orientation of the end effector measured relative to a coordinate system fixed to the ground for a specified set of joint variables. The result can be represented as a Transformation matrix. The reverse or inverse analysis deals with determining a set of joint variables that will position and orient the end effector as desired. The forward analysis of serial manipulators is quite simple and straightforward while the reverse analysis is very complex and often requires the solution of multiple non-linear equations to obtain multiple solution sets [2]. On the other hand, for parallel manipulators, the reverse analysis is straightforward while the forward position analysis is complicated. This kind of phenomenon is usually referred to as serial-parallel duality.

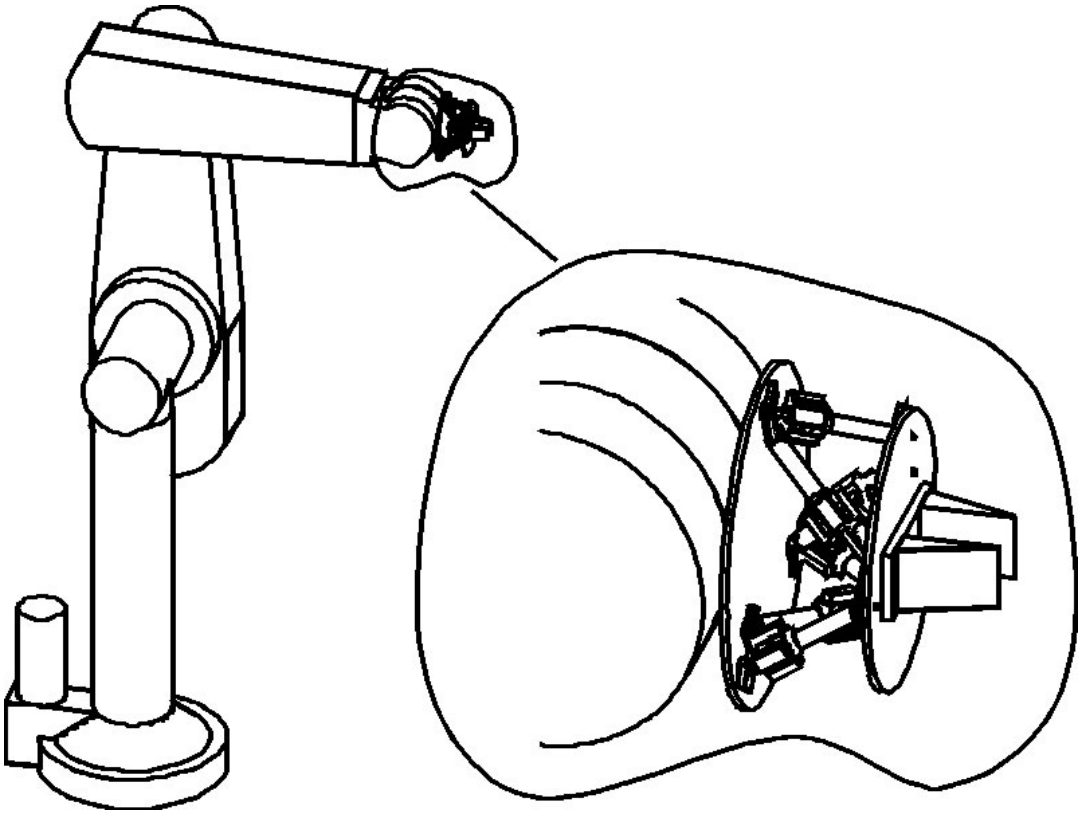

Figure 1-4. Compliant platform inserted between tool mounting plate and end effector

The first parallel spatial industrial robot is credited to Pollard's five DOF parallel spray painting manipulator that had three branches. This manipulator was never actually built. In the late 1950s, Dr. Eric Gough invented the first well-known octahedral hexapod with six struts symmetrically forming an octahedron called the universal tire-testing machine in response to the problem of aero-landing loads. Then in 1965, Stewart published his paper on the design of a parallel-actuated mechanism as a six-DOF flight simulator. It's widely referred to as the "Stewart platform". Stewart's paper gained much attention and had a great impact on the subsequent development of parallel mechanisms. Since then, much work has been done in the field of parallel geometry and kinematics such as geometric analysis, kinematics and statics and parallel dynamics and controls. In addition to theoretical studies, experimental works on prototypes of the Stewart platform have also been conducted for studying its properties and performance. The fine positioning and orienting capability of the Stewart platform make it very suitable for use in control applications as dexterous wrists and various constructions of Stewart platform based wrists.

The most commonly used 6-DOF parallel mechanism consists of two rigid bodies connected through six identical leg connectors with six extensible legs each with spherical joints at both ends or with a spherical joint at one end and a universal joint at the other. This geometric arrangement is also known as a 6-6 Parallel Kinematic Mechanism (PKM) or "6-6 platform". The six joint points on the base platform are often but not necessarily located on one plane and are arranged in some symmetric pattern. Besides the general 6-6 parallel platform, there are some other configurations. One common configuration of a parallel mechanism is the 3-3 parallel manipulator as shown

in Figure 1-5. The 3-3 parallel platform also has six connector legs, but each leg shares one joint point with another leg on the base platform and similarly on the top platform. The three shared joint points form a triangle on both the planar top platform and the planar base platform.

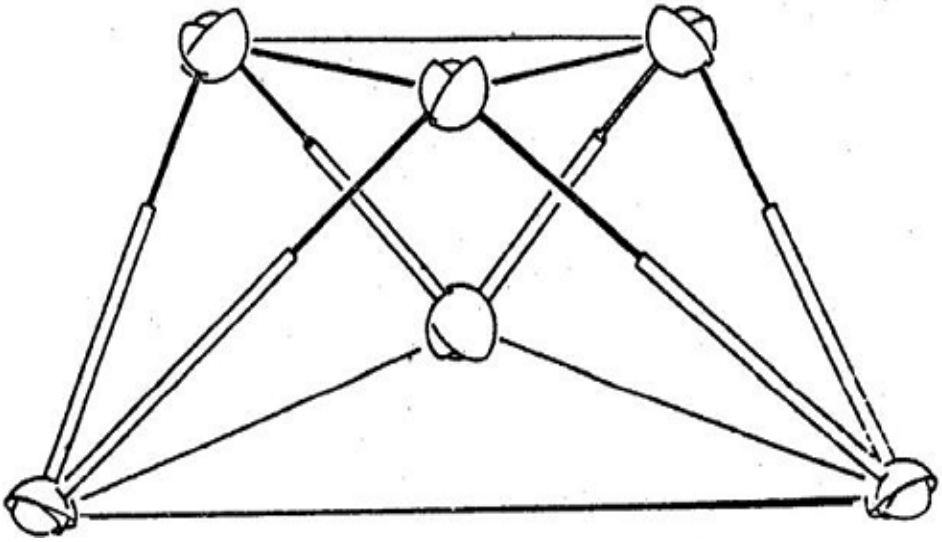

Figure 1-5. 3-3 parallel platform [8]

The mobility of a general spatial mechanism can be calculated using the following Equation 1-1

$$M = \lambda(n-1) - \sum_{i=1}^{j} (\lambda - f_i) \qquad (1\text{-}1)$$

were

M : Mobility or number of degree of freedom of the system.

λ : Degrees of freedom of the space in which a mechanism is intended to function, for the spatial case, λ = 6

n : Number of links in the mechanism, including the fixed link

j : Numbers of joints in a mechanism, assuming that all the joints are binary.

f_i : Degrees of relative motion permitted by joint i.

CHAPTER 2
THEORETICAL BACKGROUND

2.1 Forward Kinematic Analysis

In a parallel platform, usually the legs are composed of actuated prismatic joints that are connected to the top platform and base platform by a spherical joint at one end and either a spherical or universal joint at the other. The connector properties are generally referred to as the connector length or leg length as this parameter is usually measured as part of a closed-loop feedback scheme to control the prismatic actuator. Finding the position and orientation of the top platform relative to a coordinate system fixed to the base platform for a specified set of leg lengths is referred to as the forward kinematic analysis.

It has been observed that the closed-form solution for the forward kinematics problem could be simplified by regulating the connector joint locations. The simplest case is the 3-3 platform, which is degenerated by grouping the connector joints into three pairs for both the top platform and base platform; each pair of connectors shares one joint point. Although it is difficult to design a physical octahedral structure with the concentric double-spherical joints that would have sufficient loading capacity and adequate workspace due to collisions of the leg connectors themselves, the forward analysis is the simplest for this class. The forward analysis of this device was first solved by Griffis and Duffy [7] who showed how the position and orientation of the top platform can be determined with respect to the base when given the lengths of the six connectors as well as the geometry of the connection points on the top and base. The solution is a closed-form solution and is based on the analysis of the input/output relationship of three spherical four bar mechanisms. There can be up to 16 real

solutions, i.e. 8 solutions and their reflected images about the plane formed by the base connector points [7].

The geometrical method, patented by Duffy and Griffis [Gri93] for determining the equivalent 3-3 parallel structure for a special 6-6 configuration mechanism has been used for forward kinematic analysis of the parallel mechanism used in this thesis. The configuration of a special 6-6 parallel platform (as shown in Figure 2-1) was carefully chosen such that the forward kinematic analysis can use a method similar to the method for the 3-3 parallel platform. Each of the six legs is a Spherical-Prismatic-Hooke (SPH) chain which connects the mobile top and fixed base platforms. The relationship between this Special 6-6 platform and its equivalent 3-3 platform was discovered by Griffis and Duffy.

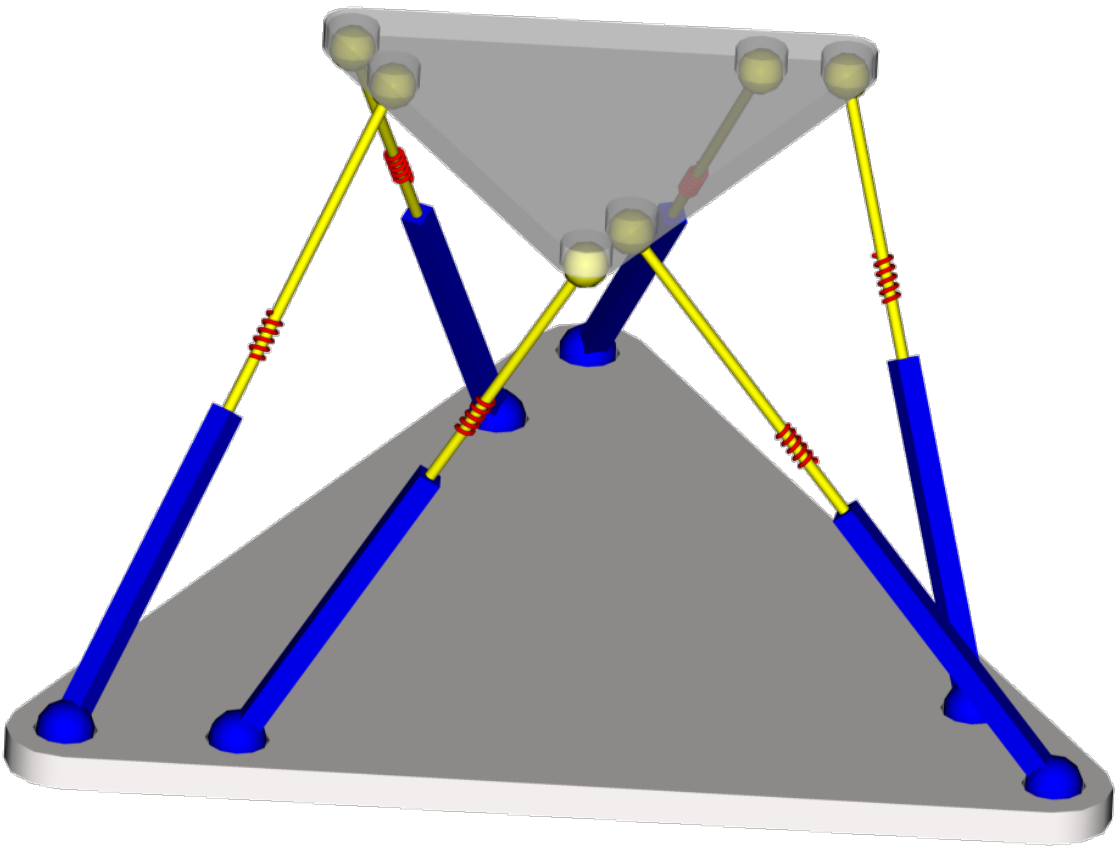

Figure 2-1. The Special 6-6 platform

A Special 6-6 platform is defined as one which is geometrically reducible to an equivalent 3-3 platform. Figures 2-2 and 2-3 depict a perspective and plan view of the 6-6 platform respectively where the leg connector points R_0, S_0 and T_0 lie along the edges of the triangle defined by points O_0, P_0 and Q_0 and the leg connector points O_1, P_1 and Q_1 lie along the edges of the triangle defined by the points R_1, S_1 and T_1. The objective is to determine the distance between the pairs of points O_0 - R_1, O_0 - S_1, P_0 - S_1, P_0 -T_1, Q_0 - T_1 and Q_0 - R_1. These distances are leg lengths for an equivalent 3-3 platform.

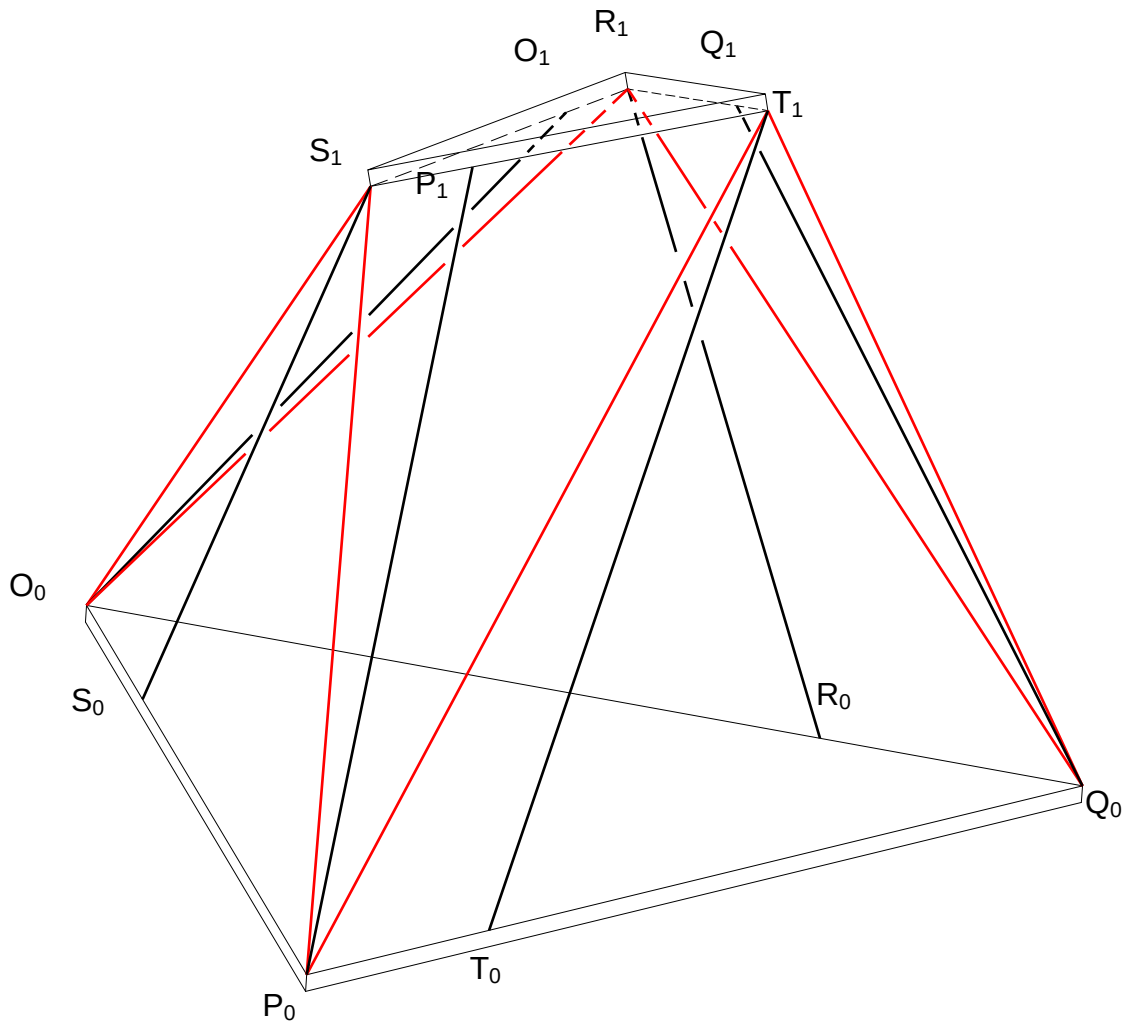

Figure 2-2. Perspective view of the special 6-6 platform

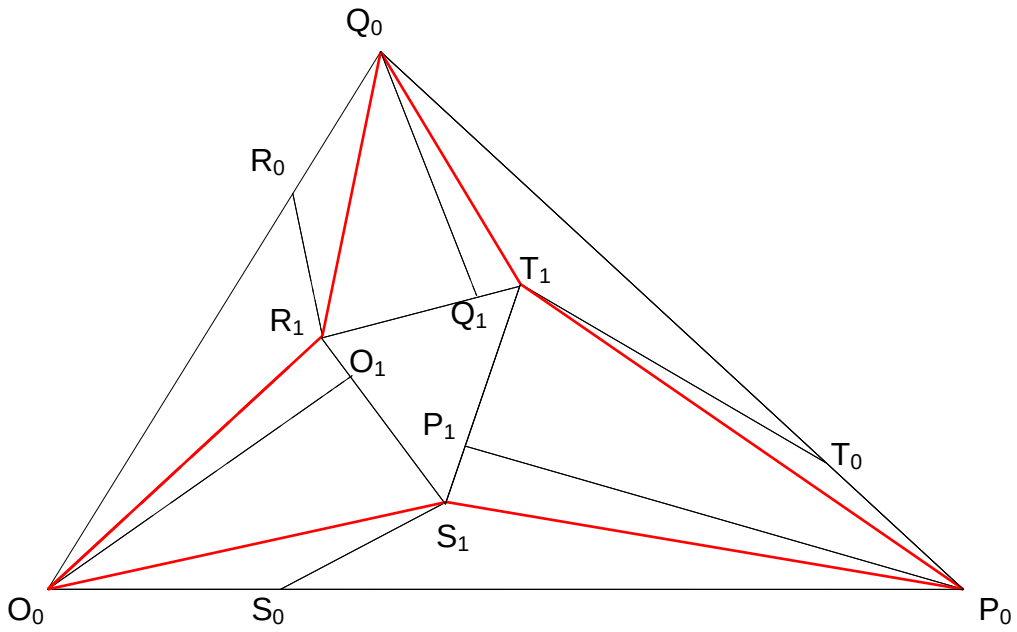

Figure 2-3. Plan view of special 6-6 platform

Throughout this analysis, the notation m_in_j will be used to represent the distance between the two points M_i and N_j and the notation $\mathbf{m_in_j}$ will represent the vector from point M_i to N_j. Using this notation, the problem statement can be written as:

Given: o_0o_1, p_0p_1, q_0q_1, r_0r_1, s_0s_1, t_0t_1 ; *connector lengths for Special 6-6 platform*

o_0p_0, p_0q_0, q_0o_0, o_0s_0, p_0t_0, q_0r_0 ; *base triangle parameters*

r_1s_1, s_1t_1, t_1r_1, r_1o_1, s_1p_1, t_1q_1 ; *top triangle parameters*

Find: o_0r_1, o_0s_1, p_0s_1, p_0t_1, q_0t_1, q_0r_1 ; *connector lengths for equivalent 3-3 platform*

Obviously it is the case that

$$s_0p_0 = o_0p_0 - o_0s_0 \;\; ; \;\; t_0q_0 = p_0q_0 - p_0t_0 \;\; ; \;\; r_0o_0 = q_0o_0 - q_0r_0$$

$$o_1s_1 = r_1s_1 - r_1o_1 \;\; ; \;\; p_1t_1 = s_1t_1 - s_1p_1 \;\; ; \;\; q_1r_1 = t_1r_1 - t_1q_1 \qquad (2\text{-}1)$$

Once the leg length dimensions of the equivalent 3-3 platform are determined, the forward analysis of the 3-3 device is used to determine the position and orientation of the top platform relative to the base.

2.2 Forward and Reverse Static Analysis

The concept of wrench from screw theory, which was introduced by Ball is employed to describe a force/torque applied to a body [1]. The forward static analysis consists of computing the resultant wrench $\hat{\mathbf{w}} = \{\mathbf{f}; \mathbf{m_0}\}$ due to the six forces generated in the legs acting upon the top platform. Now $\hat{\mathbf{w}}$ can be expressed in the form

$$\hat{\mathbf{w}} = \{\mathbf{f_1}; \mathbf{m_{01}}\} + \{\mathbf{f_2}; \mathbf{m_{02}}\} + ... + \{\mathbf{f_6}; \mathbf{m_{06}}\} \tag{2-2}$$

or

$$\hat{\mathbf{w}} = f_1\{\mathbf{S_1}; \mathbf{S_{0L1}}\} + f_2\{\mathbf{S_2}; \mathbf{S_{0L2}}\} + ... + f_6\{\mathbf{S_6}; \mathbf{S_{0L6}}\} \tag{2-3}$$

where $\{\mathbf{S}_i; \mathbf{S}_{0\mathbf{L}i}\}, i = 1...6$ are the Plücker coordinates of the line along the six legs. Refer to Appendix - A for coordinates of a line. It is convenient to express (2-2) in the form

$$\hat{\mathbf{w}} = f_1\begin{bmatrix} \mathbf{S_1} \\ \mathbf{S_{0L1}} \end{bmatrix} + f_2\begin{bmatrix} \mathbf{S}_2 \\ \mathbf{S_{0L}}2 \end{bmatrix} + ... + f_6\begin{bmatrix} \mathbf{S}_6 \\ \mathbf{S_{0L}}6 \end{bmatrix} \tag{2-4}$$

which may again be written as

$$\hat{\mathbf{w}} = \mathbf{j}\,\boldsymbol{\lambda} \tag{2-5}$$

where $\mathbf{j}$ is a 6 x 6 matrix called as the Jacobian matrix and is given as

$$\mathbf{j} = \begin{bmatrix} \mathbf{S_1} & \mathbf{S_2} & \mathbf{S_3} & \mathbf{S_4} & \mathbf{S_5} & \mathbf{S_6} \\ \mathbf{S_{0L1}} & \mathbf{S_{0L2}} & \mathbf{S_{0L3}} & \mathbf{S_{0L4}} & \mathbf{S_{0L5}} & \mathbf{S_{0L6}} \end{bmatrix} \tag{2-6}$$

and $\boldsymbol{\lambda}$ is a column vector given as

$$\boldsymbol{\lambda} = \begin{bmatrix} f_1 \\ f_2 \\ f_3 \\ f_4 \\ f_5 \\ f_6 \end{bmatrix} \tag{2-7}$$

$\mathbf{j}$ maps the force magnitudes along each leg to the externally applied wrench.

The geometry of the platform i.e. the position and orientation of the top platform relative to the base is solved first and hence, the six columns of $\mathbf{j}$ are known. Furthermore, the magnitude $f_i, i = 1...6$ for each of the leg force is known. Then, the resultant wrench can be computed from (2-5). Clearly for equilibrium, an external wrench with an equal and opposite magnitude $|\mathbf{f}|$ must be applied to the platform.

Conversely, when the position and orientation of the top platform is know relative to the base and an external wrench or force is applied to the top platform, it is required to determine the magnitudes $f_i, i = 1...6$ of the connector forces. This is called the reverse or inverse static analysis. This is accomplished by solving for $\boldsymbol{\lambda}$ as

$$\boldsymbol{\lambda} = \mathbf{j}^{-1}\ \hat{\mathbf{w}} \qquad (2\text{-}5)$$

where $\mathbf{j}^{-1}$ is the inverse of $\mathbf{j}$.

The computation cannot be performed when the rank of $\mathbf{j}$ is less than six for which the Plücker coordinates of the lines along the six legs become linearly dependant and the platform gets into a singular position [1]

2.3 Compliance Analysis

A derivative of the above Equation 2-5 will yield a relationship between the changes in individual leg forces to the change in the externally applied wrench. Griffis [8] extended this analysis to show how the change in the externally applied wrench could be mapped to the instantaneous motion of the top platform. According to the static force analysis presented above, it is straightforward to design a compliant parallel platform to detect forces and torques. Once the forward position analysis is completed to determine the current pose, the knowledge of the stiffness constant and free length of

each connector and measurement of the current leg lengths allows for the computation of the external wrench.

Based on this relationship, Griffis and Duffy introduced the theory of kinestatic control to simultaneously control force and displacement for a certain constrained manipulator based on the general spatial stiffness of a compliant coupling. [9] In their theoretical analysis of the compliant control strategy, a model of a passive Stewart platform with compliant legs was utilized to describe the spatial stiffness of the parallel platform based wrench sensor. Compared to the open loop Remote Center Compliance (RCC) compensators that are commercially available (see Figure 1-1, 2-4 and 2-5), the Stewart-platform-based force-torque sensor can provide additional information about the external wrench to assist force and position control.

Figure 2-4. ATI industrial automation 9116 series RCC compensator

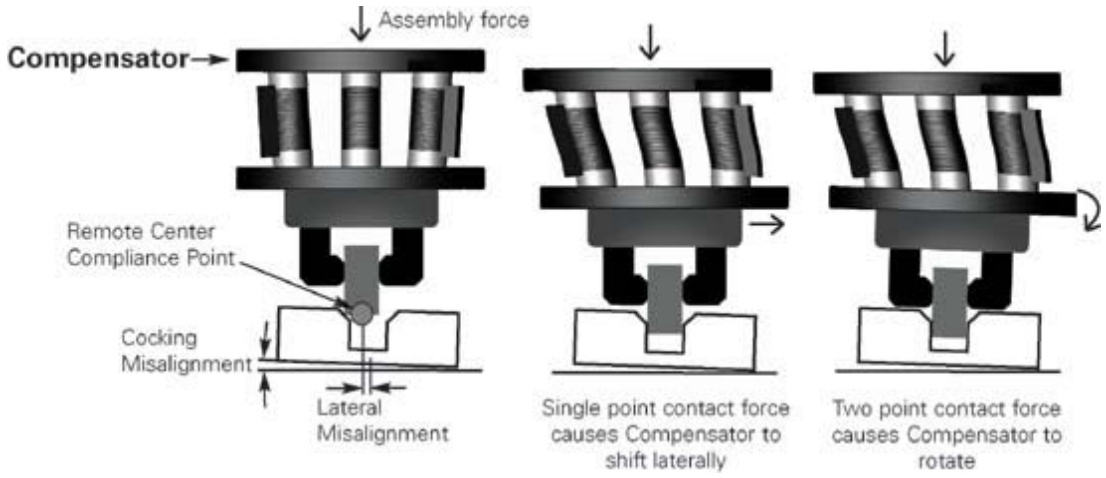

Figure 2-5. ATI industrial automation 9116 Series RCC compensatoris designed to be used in "peg-in-hole"-type operations.

Dwarakanath and Crane studied a Stewart platform based wrench sensor, using a LVDT (Linear Variable Displacement sensor) and using a potentiometer with slider crank mechanism to convert axial deflection of the spring to angular deflection. [3]

The theory of screws is a very powerful tool to investigate the compliance or stiffness characteristic of a compliant device. Ball first introduced the theory and used it to describe the general motion of a rigid body. He presented the idea of the principal screw of a rigid body, where a wrench applied along a principal screw of inertia generates a twist on the same screw. Duffy analyzed planer parallel spring systems theoretically. [4] Griffis and Duffy studied the non-symmetric stiffness behavior for a special octahedron parallel platform with 6 springs as the connectors and the stiffness mapping could be represented by a 6 x 6 matrix called Stiffness Matrix. [9]

For a compliant component, such as a spring the basic property is its stiffness. Theoretically, no object is infinitely stiff; the only difference between a so called “stiff component” and “compliant device” is that comparing with the “compliant” component, the “stiff” component has a relatively much higher rigidity or stiffness. The spring is the

most commonly used compliant component. The stiffness property of a spring is usually quantified by a ratio called the spring constant, also known as the elastic coefficient or stiffness coefficient and is used to describe compliant devices.

2.3.1 Simple Planar Case Stiffness Analysis

Hooke's Law describes the fundamental relationship between an external force and the compliant displacement in static equilibrium.

$$F_S = -k\ \Delta l = -k(l - l_0) \tag{2-5}$$

where F_S is the force exerted on the spring (or more generally, the compliant component), k is the spring constant, l is the instantaneous length of the spring, l_0 is the free length and Δl is the change in length of the spring.

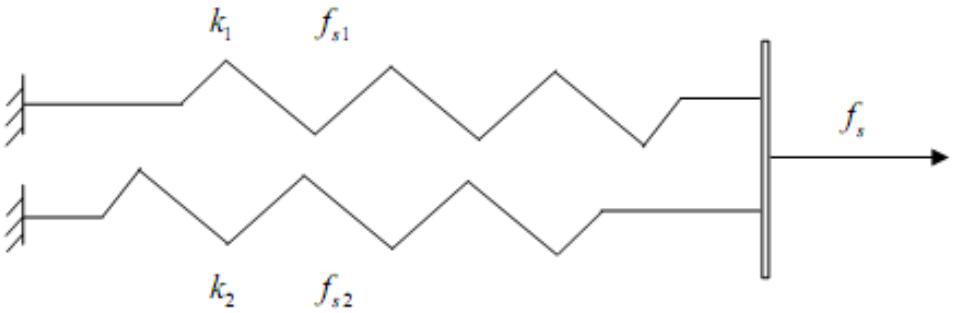

Figure 2-6. Planar in-parallel springs

Consider two springs connected in-parallel, with spring constants k_1 and k_2 respectively. An external force is applied on the right end of the two springs and in the direction along the axes of the springs. (Figure 2-6)

The force in each spring can be calculated as $F_{S1} = -k_1\ \Delta l_1$ and $F_{S2} = -k_2\ \Delta l_2$ but $\Delta l_1 = \Delta l_2 = \Delta l$. Hence, the total force applied is sum of the two spring forces and can be written as

$$F_S = F_{S1} + F_{S2} = -(k_1 + k_2)\Delta l = -k_p \Delta l \tag{2-6}$$

where k_p is the equivalent stiffness/spring constant of the in-parallel connected springs. It is the sum of the individual spring constants. This shows that when compliant components are connected in-parallel, the overall equivalent stiffness is much higher than the stiffness of any individual compliant component.

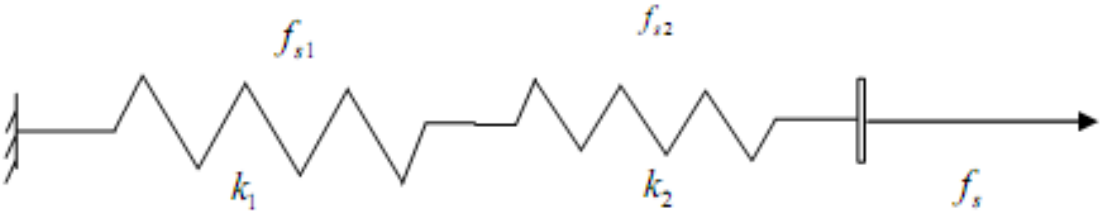

Figure 2-7. Planar serially connected springs

Now let's consider two springs connected in series. The axes of the two springs are collinear and they are connected end to end. The direction of the external force applied on them is also along the axes of the springs. (Figure 2-7). The total force can be shown as same as the forces felt by each spring $F_{S1} = -k_1\ \Delta l_1$ and $F_{S2} = -k_2\ \Delta l_2$. Here, $\Delta l = \Delta l_1 + \Delta l_2$. Hence, the total force can be written as

$$F_S = F_{S1} = F_{S2} = -k_s \Delta l = -k_s(\Delta l_1 + \Delta l_2) \tag{2-7}$$

Where k_s is the given by $\frac{1}{k_s} = \frac{1}{k_1} + \frac{1}{k_2}$ and is called the as equivalent stiffness /spring constant of the serially connected springs. Its reciprocal value is the sum of the reciprocal values of the individual spring constants. This means that when compliant components are connected serially, the overall equivalent stiffness is less than the stiffness of any individual compliant component.

For $k_1 = k_2 = k$, $k_s = \frac{k}{2}$ and if $k_1 << k_2, k_s \cong k_1$. This shows that serially connected components with widely different spring constants, have an equivalent stiffness, which is more dependent on the component with the smaller stiffness /spring constant.

According to this result, if one compliant component is connected to a relatively stiff bar, the equivalent stiffness of this two-component system is very close to the stiffness of the compliant component. The systems discussed above have one Degree of Freedom (DOF). A more general planar case would have two or more DOF.

Figure 2-8 shows a planar 2 DOF spring case. In this spring system, two translational springs are connected at one end P and grounded separately at pivot points A and B respectively. Here translational springs behave like prismatic joints in revolute-prismatic-revolute (RPR) serial chains. In the X-Y plane, two such springs form a simple compliant coupling. The two-spring compliant coupling system is equivalent to a planar two-dimensional spring. The spring is two-dimensional because two independent forces act in the translational spring, and it is planar since the forces remain in a plane. The external force applied at point P is in static equilibrium with the forces acting in the springs. The two-dimensional spring remains in quasi-static equilibrium as the point P moves gradually.

In order to analyze the two-dimensional force/displacement relationship or mapping of stiffness, it is necessary to decompose both the external force and displacements into standard Cartesian coordinate vectors. The locations of points A, B, and P, the initial and current lengths of AP and BP and the angles θ_1 and θ_2 are known. The free length of AP is l_{01} and the free length of BP is l_{02}. The spring constants are k_1

and k_2. The current length of AP and BP are l_1 and l_2 respectively. To simplify the equations, dimensionless parameters $\rho_1 = \frac{l_{01}}{l_1}$ and $\rho_2 = \frac{l_{02}}{l_2}$ are introduced. By definition, these two scalar values are always positive, and no negative spring lengths are allowed. When $\rho_i > 1$, the corresponding spring is elongated, and if $\rho_i < 1$, then it is compressed.

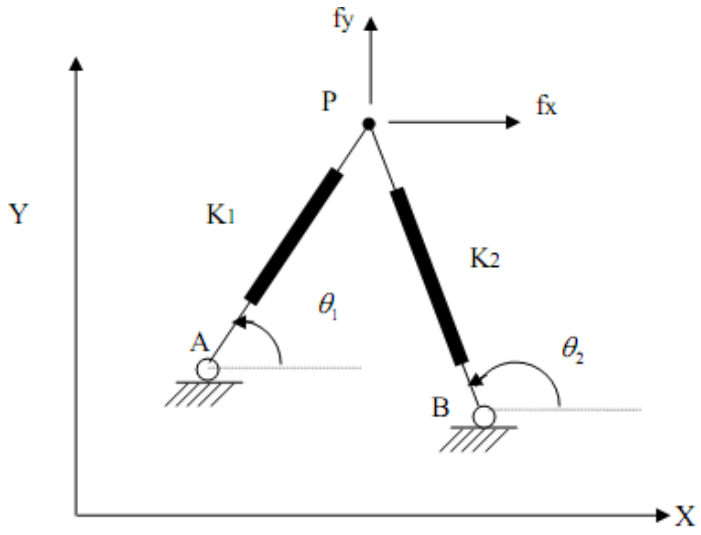

Figure 2-8. Planar 2 DOF spring

The external force applied on the spring system is given by:

$$\begin{bmatrix} f_x \\ f_y \end{bmatrix} = \begin{bmatrix} c_1 & c_2 \\ s_1 & s_2 \end{bmatrix} \begin{bmatrix} k_1(1-\rho_1)l_1 \\ k_2(1-\rho_2)l_2 \end{bmatrix} \tag{2-8}$$

Where $c_i = \cos(\theta_i)$ and $s_i = \sin(\theta_i)$. Differentiating the above Equation 2-8 will result in the following Equation 2-9

$$\begin{bmatrix} \delta f_x \\ \delta f_y \end{bmatrix} = [k] \begin{bmatrix} \delta x \\ \delta y \end{bmatrix} \tag{2-9}$$

Where $[k]$ is the mapping of the stiffness of the system and according to Griffis can be written as [8]

$$[k]=\begin{bmatrix} k_{11} & k_{12} \\ k_{21} & k_{22} \end{bmatrix}=\begin{bmatrix} c_1 & c_2 \\ s_1 & s_2 \end{bmatrix}\begin{bmatrix} k_1 & 0 \\ 0 & k_2 \end{bmatrix}\begin{bmatrix} c_1 & s_1 \\ c_2 & s_2 \end{bmatrix} + \begin{bmatrix} -s_1 & -s_2 \\ c_1 & c_2 \end{bmatrix}\begin{bmatrix} k_1(1-\rho_1) & 0 \\ 0 & k_2(1-\rho_2) \end{bmatrix}\begin{bmatrix} -s_1 & c_1 \\ -s_2 & c_2 \end{bmatrix} \tag{2-10}$$

The Spring Stiffness Matrix $[k]$ can be written in the form

$$[k]=[j][k_i][j]^T+[\delta\ j][k_i(1-\rho_i)][\delta\ j]^T \tag{2-11}$$

where $[j]$ is the static Jacobian matrix of the system, $[\delta\ j]$ is the differential matrix with respect to θ_1 and θ_2 while $[k]$ and $[k(1-\rho_i)]$ are 2 x 2 diagonal matrices. In general, $\theta_1 \neq \theta_2$ because if the two angles are equal then the spring matrix expression becomes singular. For such a case, the two springs are parallel and Equation 2-6 can be applied instead of Equation 2-10.

The concept of twist from screw theory, which was introduced by Ball is employed to describe a small (or instantaneous) displacement of a rigid body. In order to maintain the system equilibrium, the top platform moves as the external wrench changes. In general, the mapping of stiffness is a one-to-one correspondence that associates the twist describing the relative displacement between the bodies with the corresponding resultant wrench which interacts between them. This relationship is given by

$$\delta\hat{w}=[\mathbf{K}]\,\delta\hat{D} \tag{2-12}$$

The detailed derivation process was done by Duffy [4]; only the result has been shown here. $[\mathbf{K}]$ is the compliance matrix, $\delta\hat{\mathrm{w}}=[\delta\mathbf{f};\delta\mathbf{m}]^{\mathrm{T}}$ is the change of the wrench, and $\delta\hat{\mathrm{D}}=[\delta\mathbf{X};\delta\boldsymbol{\varphi}]^{\mathrm{T}}$ is the change in position and orientation.

2.3.2 Stiffness Analysis for 3-D spatial systems

Complaint Mechanisms can be considered as spatial springs with multiple DOF rather than one as linear spring have. Equation (2-12) can also be used for spatial structures. It was first shown by Griffis that the compliance matrix for the special 6-6 parallel mechanism may be written as the sum of five matrices as [8]

$$[\mathbf{K}] = [\mathbf{j}][k_i][\mathbf{j}]^T + [\delta\mathbf{j}_\theta][k_i(1-\rho_i)][\delta\mathbf{j}_\theta]^T + [\delta\mathbf{j}_\alpha][k_i(1-\rho_i)][\delta\mathbf{j}_\alpha]^T + [\delta\mathbf{j}_\theta][k_i(1-\rho_i)][V_\theta]^T + [\delta\mathbf{j}_\alpha][k_i(1-\rho_i)][V_\alpha]^T \quad (2\text{-}13)$$

where $[\mathbf{j}]$ is a 6 x 6 matrix whose columns are the Plücker coordinates of the lines along the six leg connectors and $[k_i]$ is a diagonal 6 x 6 matrix whose diagonal elements are the spring constants of the six leg connectors. The term ρ_1 is defined as

$$\rho_i = \frac{\ell_{0i}}{\ell_i} \quad (2\text{-}14)$$

which is the ratio of the free length of connector i to the current length of the connector and the term $[k_i(1-\rho_i)]$ is a diagonal 6 X 6 matrix whose diagonal elements are given by $k_i(1-\rho_i)$ The terms $[\delta\mathbf{j}_\theta]$ and $[\delta\mathbf{j}_\alpha]$ are each 6×6 matrices whose columns are the derivatives of the Plücker coordinates of the lines along the leg connectors taken with respect to θ_i and α_i which are angles which define the direction of the line along leg i. The remaining terms to be defined in Equation 2-13 are $[V_\theta]$ and $[V_\alpha]$.

Next, six unit vectors are defined as intermediate variables describing the directional information of the base platform triangle sides as

$$\mathbf{u_1} = \frac{-\mathbf{EA}}{\|\mathbf{EA}\|}, \mathbf{u_2} = \frac{\mathbf{AC}}{\|\mathbf{AC}\|}, \mathbf{u_3} = \frac{-\mathbf{AC}}{\|\mathbf{AC}\|}, \mathbf{u_4} = \frac{-\mathbf{EC}}{\|\mathbf{EC}\|}, \mathbf{u_5} = \frac{\mathbf{EC}}{\|\mathbf{AC}\|}, \mathbf{u_6} = \frac{\mathbf{EA}}{\|\mathbf{EA}\|} \quad (2\text{-}15)$$

$\mathbf{V_i}$ is given by the expression

$$\mathbf{V_i} = \frac{\mathbf{u_i} \times \mathbf{S_i}}{\left\| \mathbf{u_i} \times \mathbf{S_i} \right\|} \tag{2-16}$$

$$\boldsymbol{\delta}\mathbf{S_i}^{\boldsymbol{\theta}} = \mathbf{V_i} \quad and \quad \boldsymbol{\delta}\mathbf{S_i}^{\alpha} = \mathbf{V_i} \times \mathbf{S_i} \tag{2-17}$$

$$[V_\alpha] = \begin{bmatrix} 0 & 0 & 0 & 0 & 0 & 0 \\ l_1\,\mathbf{V_1} & l_2\,\mathbf{V}_2 & l_3\,\mathbf{V}_3 & l_4\,\mathbf{V}_4 & l_5\,\mathbf{V}_5 & l_6\,\mathbf{V}_6 \end{bmatrix} \tag{2-18}$$

$$[V_\theta] = \begin{bmatrix} 0 & 0 & 0 & 0 & 0 & \mathbf{0} \\ l_1\,\mathbf{S_1} \times \mathbf{V_1} & l_2\,\mathbf{S}_2 \times \mathbf{V}_2 & l_3\,\mathbf{S}_3 \times \mathbf{V}_3 & l_4\,\mathbf{S}_4 \times \mathbf{V}_4 & l_5\,\mathbf{S}_5 \times \mathbf{V}_5 & l_6\,\mathbf{S}_6 \times \mathbf{V}_6 \end{bmatrix} \tag{2-19}$$

Substituting all the necessary components in Equation 2-13 yields the global stiffness matrix of the special 6-6 parallel passive mechanism via the stiffness mapping analysis.

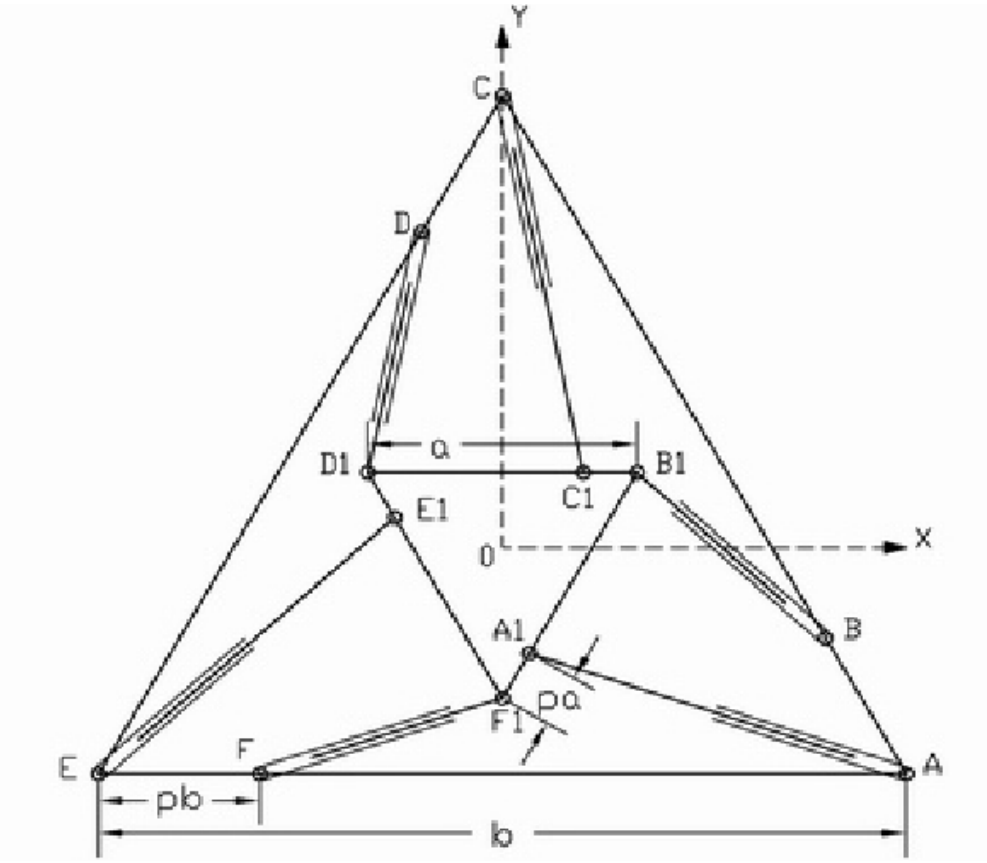

Figure 2-9. Top view of the special 6-6 configuration

2.3.3 Theory of Kinestatic Control

The theory of Kinestatic Control was proposed by Griffis and Duffy in 1991. [9] In general, the spatial stiffness of a compliant coupling that connects a pair of rigid bodies is used to map a small twist between the bodies into the corresponding interactive wrench. This mapping is based upon a firm geometrical foundation and establishes a positive-definite inner product (elliptic metric) that decomposes a general twist into a twist of freedom and a twist of compliance.

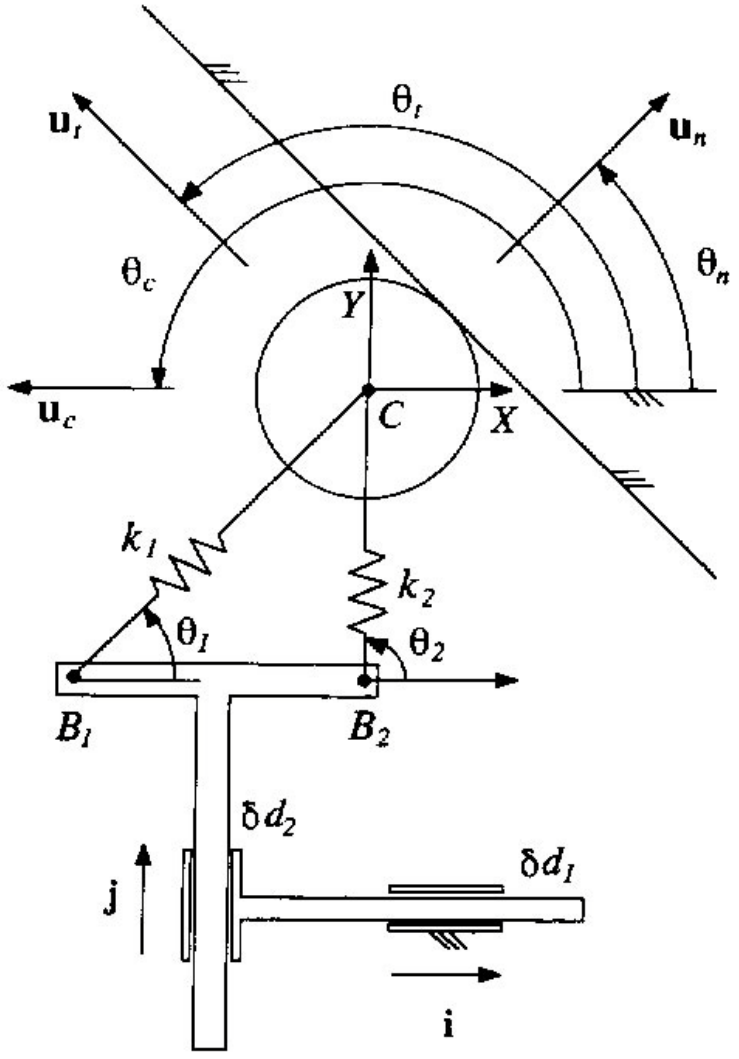

Figure 2-10. Passive compliance device for contact force control

A planar example is shown in Figure 2-10. A serial pair of actuated prismatic joints supports a wheel via a two-spring system. The actuated prismatic joints are controlled so that the wheel can maintain a desired contact with a rigid wall. [8] [4] The objective of this simple example is to control the contact force between the wheel and the rigid wall when the wheel is sliding along the surface. The serial pair of actuated prismatic joints supports the body B_1B_2, which connects with the wheel via two compliant connectors (B_1C and B_2C). The actuator drives the body with pure motion in the i and j directions to adjust the position of the wheel along the surface and the contact force between the wheel and the surface.

Given the compliant proprieties of the two connectors (spring constants k_1 and k_2 and free lengths L_{01} and L_{02} for B_1C and B_2C respectively) and the geometry of the mechanism (angle θ_1 and θ_2), the control objective is to determine the displacement changes for the two prismatic actuators, i.e. δd_1 and δd_2 in order to achieve a desired position of the wheel and contact force between the wheel and the surface.

A significant result of this work was that Griffis and Duffy proved that the instantaneous compliance matrix which relates a change in the applied wrench (force for the planar example) to the relative displacement of the compliant mechanism was not symmetric when an external wrench was applied across the compliant mechanism. It was shown that the change in force is related to change in position by the following Equation 2-20

$$\begin{bmatrix} \delta f_x \\ \delta f_y \end{bmatrix} = [\mathbf{K}] \begin{bmatrix} \delta x \\ \delta y \end{bmatrix} \tag{2-20}$$

Where $[\mathbf{K}]$ is the Compliance Matrix of the system and can be written as

$$[\mathbf{K}] = \begin{bmatrix} k_{11} & k_{12} \\ k_{21} & k_{22} \end{bmatrix} = \begin{bmatrix} c_1 & c_2 \\ s_1 & s_2 \end{bmatrix} \begin{bmatrix} k_1 & 0 \\ 0 & k_2 \end{bmatrix} \begin{bmatrix} c_1 & s_1 \\ c_2 & s_2 \end{bmatrix} \tag{2-21}$$

By knowing the Compliance Matrix, the manipulator can do a pure position move of the end effector in order to control the position of the wheel along the wall and the contact force with the wall.

To apply Kinestatic control to the general spatial case, it is necessary that the compliant mechanism possess six degrees of freedom. One implementation of the device is the special 6-6 parallel platform in which the joints in the leg connectors are passive, i.e. there are no actuators. Recollecting from the description of the Special 6-6 parallel platform from section 2-1, each leg connector is a SPH serial chain which means each leg is made up of series of links connected by a spherical joint followed by a prismatic joint followed by a Hooke joint. The prismatic joint will be compliant and the spring constant and free length of each connector is assumed to be known. Such a device can be inserted between the tool mounting plate of a six degree of freedom industrial manipulator and the end effector tooling as shown in Figure 1-4. By instrumenting each of the six leg connectors so that the length of each connector can be measured, then the force in each connector and thereby the wrench currently applied to the top platform can be determined. The objective then is to determine how the industrial manipulator should change the position and orientation of the tool mounting plate (attached to the base platform) so that the external wrench that is being experienced at the top platform is as desired. The whole closed loop process scheme has been shown in Figure 2-11.

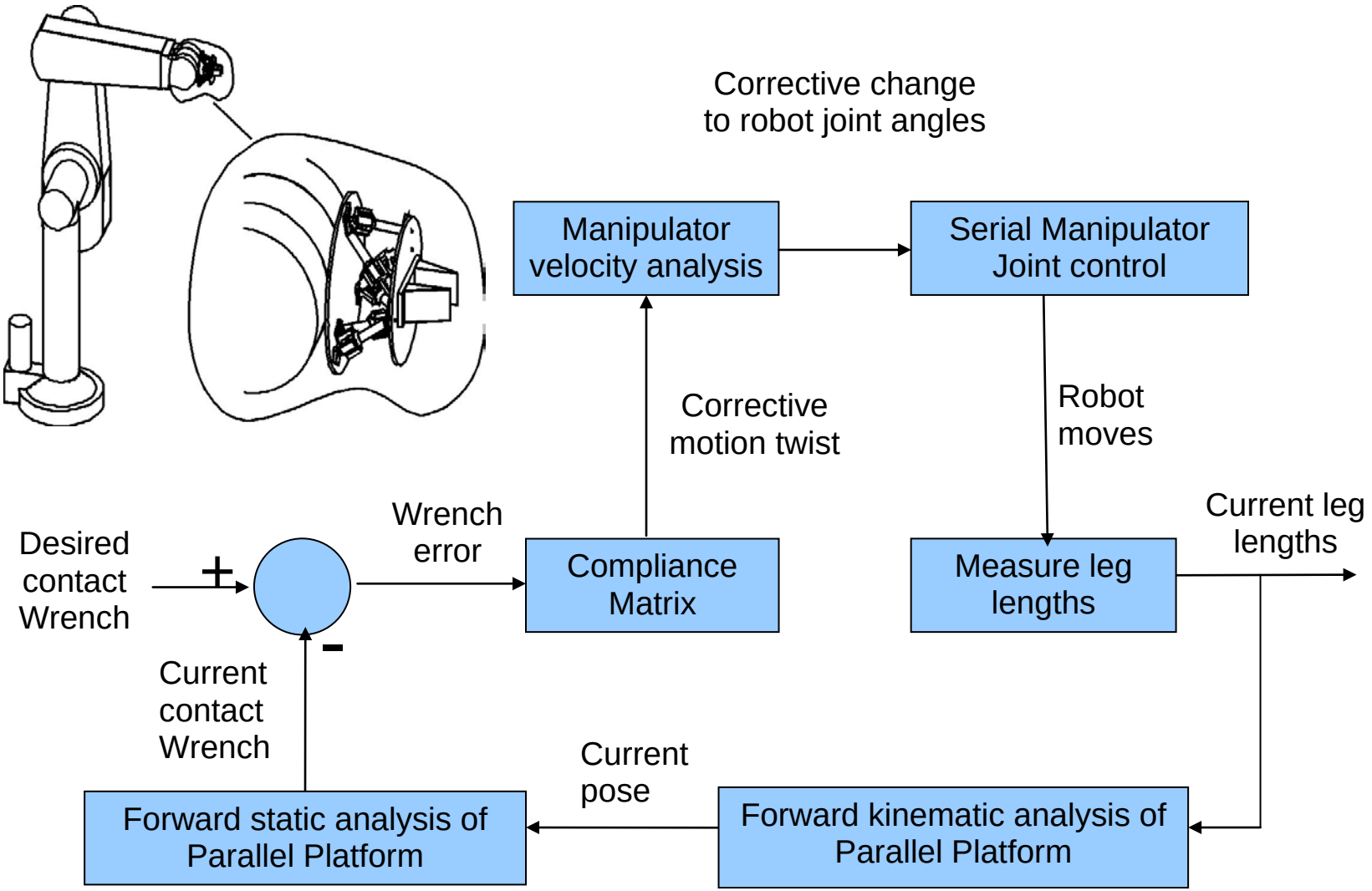

Figure 2-11. Kinestatic control: closed loop process scheme

CHAPTER 3
MECHANICAL DESIGN OF THE PARALLEL PLATFORM

In this chapter, the mechanical design of the prototype of the force compliant parallel platform is discussed. The mechanical design of the prototype was done by Bo Zhang and this formed the basis for the Electrical Design and Implementation. [12]

3.1 Design Specifications

The device's geometrical and functional requirements are stated as follows:

SP1. The mechanism should be compliant in nature to measure contact loads

SP2. The mechanism should have six degrees of freedom

SP3. The mechanism should be a spatial parallel device

SP4. The mechanism should be able to measure loads without large errors

SP5. The device should have a relatively compact size

The 6-6 Special parallel Stewart platform is a promising structure for such a spatial compliant devices. The Stewart platform structure satisfies the SP2 and SP3 criteria. With each connector being composed of a prismatic joint as the compliant component For example – using linear springs, the SP1 and SP4 criteria could also be satisfied. One of the main advantages of the Stewart platform is that it can withstand a large payload (compared to serial geometries) with relatively compact size. As a result, the dimensional requirement - SP5 could be met during the conceptual design and physical design stage. The detailed design specifications are presented in Table 3-1. Note that in Table 3-1, the direction of the z axis is referred to as perpendicular to the plane of the base platform.

Table 3-1. Design objective specifications

Specifications	Range
Individual Connector Deflection	± 5mm
Maximum perpendicular load	50 N
Motion range in Z direction	± 4 mm
Motion range in X,Y directions	± 3.5 mm
Rotational range about Z axis	± 6°
Rotational range about X,Y axes	± 4°
Position measurement resolution	0.01 mm

3.2 Conceptual Design

A 3-3 octahedral structure (Figure 1-5) was first considered as this is geometrically simplest among all six degree of freedom parallel platform. The terminology 3-3 refers to the fact that the device has three connection points on the bottom platform and three connection points on the top platform. The 3-3 parallel platform consists of a top mobile platform, a base fixed platform, 6 connectors, and 6 concentric spherical joints, three on the base platform and three on the top platform. Although it offers the simplest forward analysis solution, the device is mechanically complex and hence, difficult to design accurately.

A general 6-6 platform avoids this mechanical design problem but the forward position analysis of this device would require solution of a 40th order polynomial. As a result, the Special 6-6 parallel platform developed by Griffis and Duffy was chosen. Here, the concentric ball and socket joints have been separated such that all the base platform connection points lie on a triangle and all the top platform connection points lie on a second triangle. The complexity of the forward analysis of this device is of the same order as that of the 3-3 device because it can be reduced to an equivalent 3-3 device based on the constant mechanism parameters and the six measured leg lengths. In order to eliminate the six additional rotational freedoms, the six spherical joints

connecting the top platform and leg connectors are replaced by universal or Hooke joints.

Equation (1-1) is utilized here to calculate the mobility of the special 6-6 parallel platform.

$$M = 6(14-1) - \sum_{i=1}^{6}(6-3) - \sum_{i=1}^{6}(6-2) - \sum_{i=1}^{6}(6-1) = 78 - 18 - 24 - 30 = 6$$

The legs 1-6 are arranged in such a way that each of them is connecting to a corner connecting point on either the top or base platform while the other connecting point is in the midline of the triangle of the opposing platform. If the midline connecting points are not exactly on the middle of the triangle side and for each side of the triangle, and the points are distributed symmetrically, there are two different configurations which are usually called “clockwise” configuration and “anti-clockwise” (the rotation direction of the top platform when pressed) configuration based on the plan view of the structure. There is no significant analytical difference between the two configurations for the kinematic analysis and control, so only one configuration is used to build the prototype. One computer generated model of these configurations is shown in Figure 3-1.

The next issue was to determine the best configuration for the top platform when the device is in its home unloaded configuration. In this analysis, ‘best’ was defined as the configuration where the Plücker coordinates of the six leg connectors are ‘as far as possible’ from being linearly dependent. Lee [10] analyzed the 3-3 and Special 6-6 platforms to determine the ratio of the size of the top platform to the base as well as the height and pose of the top platform such that the determinant of the 6 × 6 matrix formed by the Plücker coordinates of the six leg connectors would be at its maximum value. The result was that if the length of the side of the top platform triangle

was *a* then the optimal unloaded home position pose would occur if the base triangle was twice this size, i.e. 2*a*, and the top platform was parallel to the base at a distance *a* above it while rotated about the *Z* axis as shown in the configuration in Figure 3-1.

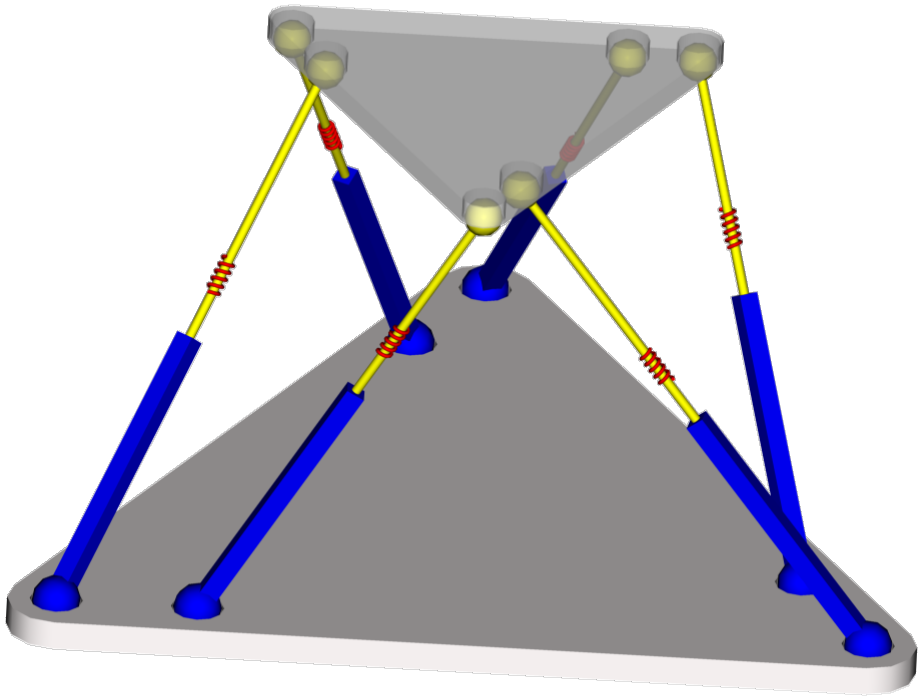

Figure 3-1. The special 6-6 platform

3.3 Prototype Design

The free lengths of the connectors are calculated by the following Equations 3-1 and 3-2:

$$l_{long} = \sqrt{\frac{1}{3}\left(3h^2 + a^2(3\rho^2 - 3\rho + 1) - (\cos\theta + \sqrt{3}(2\rho - 1)\sin\theta)ab + b^2\right)} \quad (3\text{-}1)$$

$$l_{short} = \sqrt{\frac{1}{3}\left(3h^2 + b^2(3\rho^2 - 3\rho + 1) - (\cos\theta - \sqrt{3}(2\rho - 1)\sin\theta)ab + a^2\right)} \quad (3\text{-}2)$$

As shown in Figure 3-2,

l : Free length of the legs, divided into two groups based on the fact that there are two different values for free length of the legs.

a : refers to the functional triangle edge length of the top form.

b : refers to the functional triangle edge length of the base form.

θ : refers to the rotation angle of the top platform about the z-axis.

ρa, ρb : refer to the distance between adjacent joint points on the base platform and top platform.

Zhang chose the parameters based on various factors like feasibility of manufacturing, encoders available in the market, necessary working space without interference, etc. [12] The selected values were

$$a = 60mm,\ b = 120mm,\ \rho = 28/120 = 0.2333,\ h = a = 60mm,$$
$$L_{Short} = 68.021mm,\ L_{Long} = 80.969mm \tag{3-3}$$

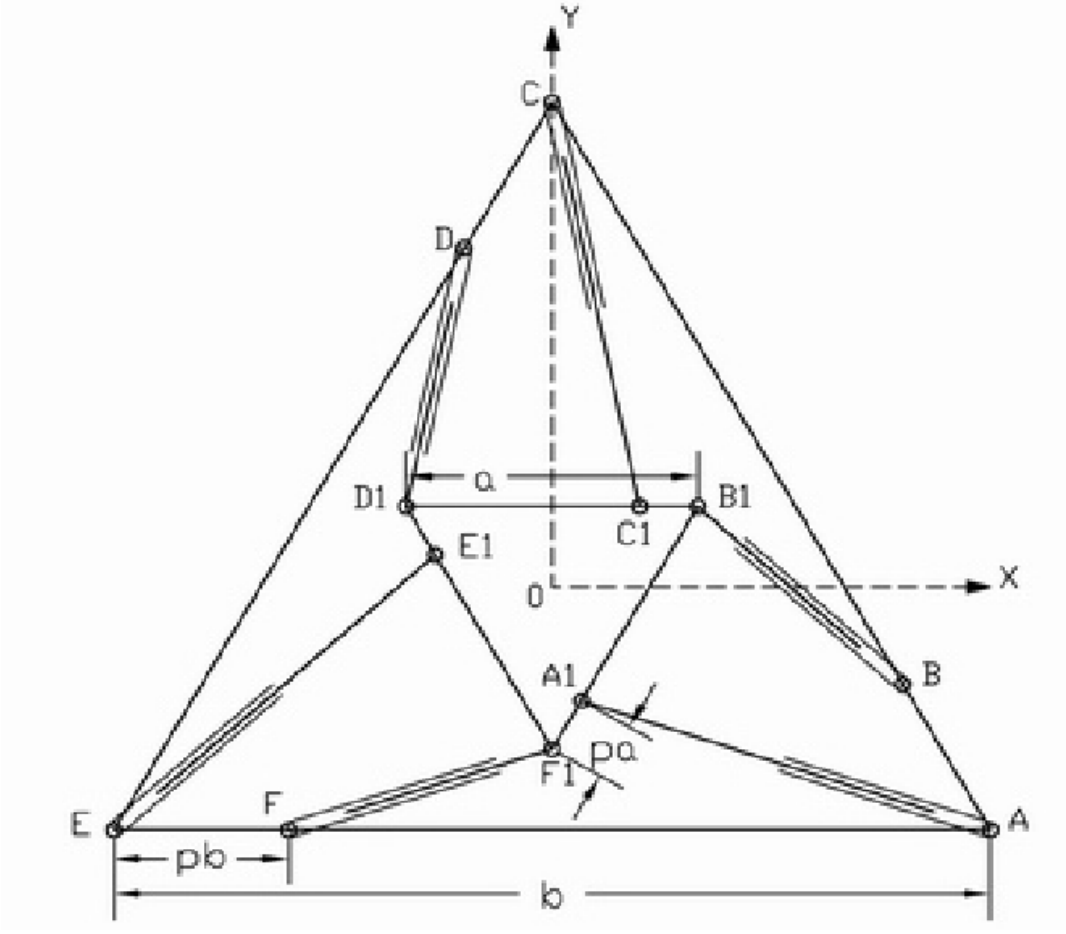

Figure 3-2. Plan view of the Special 6-6 platform

The prismatic joint on the leg is spring loaded. Precision linear springs were selected for use as the elastic component to provide elongation and compression of the leg connectors. After carefully studying and comparing different springs, Zhang chose cylindrical precision springs with spring constant 2.627 N/mm and the high linear coefficient (± 5%).[12]

The free length variation of each connector is measured by a linear optical encoder. Each leg connector is comprised of two parts that translate with respect to each other and are interconnected by the spring. The encoder read head is attached to one of the leg parts and the encoder linear scale is attached to the other. The two leg parts are constrained by a ball spline to ensure that they translate relative to one another and to help maintain alignment of the encoder read head and linear scale.

Since the six connecting points on the base platform are in the same plane, the centers of the pseudo-spherical joints are also in the same virtual plane. The free length of the connectors is defined as the distance between the two centers of the joints, which connect the connector with the top platform and the base platform. The top end of the legs were chosen to have a Hooke joint while the bottom end were chosen to have spherical joints formed using combination of bearings and Hooke joints.

Figure 3-3. Photo of leg connector (Notice the linear encoder and the joints)

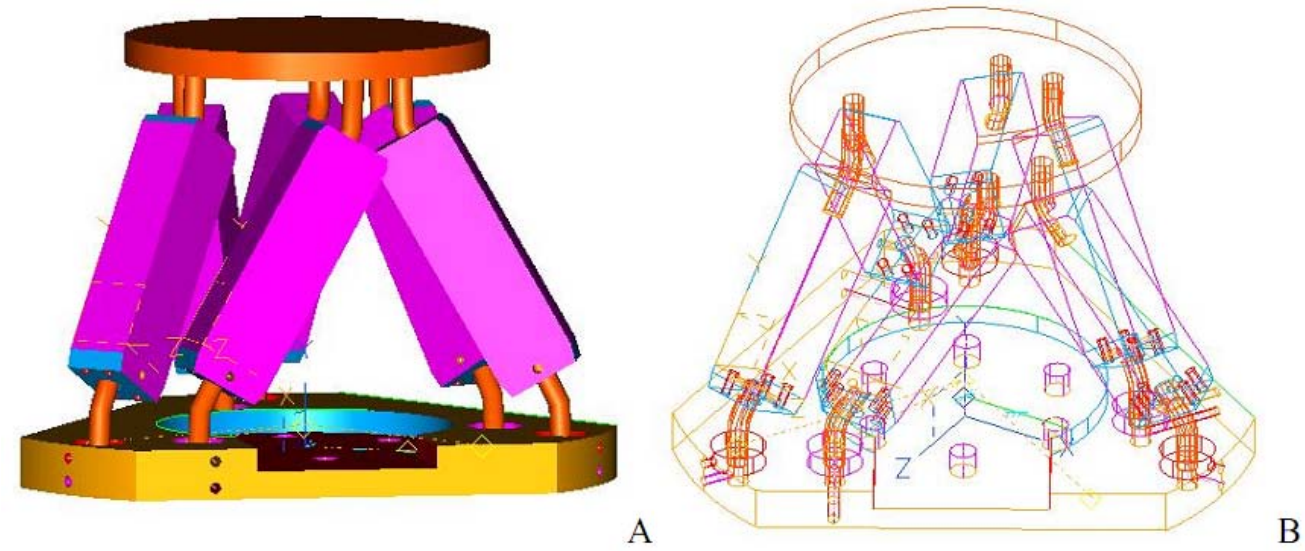

Figure 3-4. 3-D model of the special 6-6 parallel platform prototype. A) Solid model, B) Frame model.

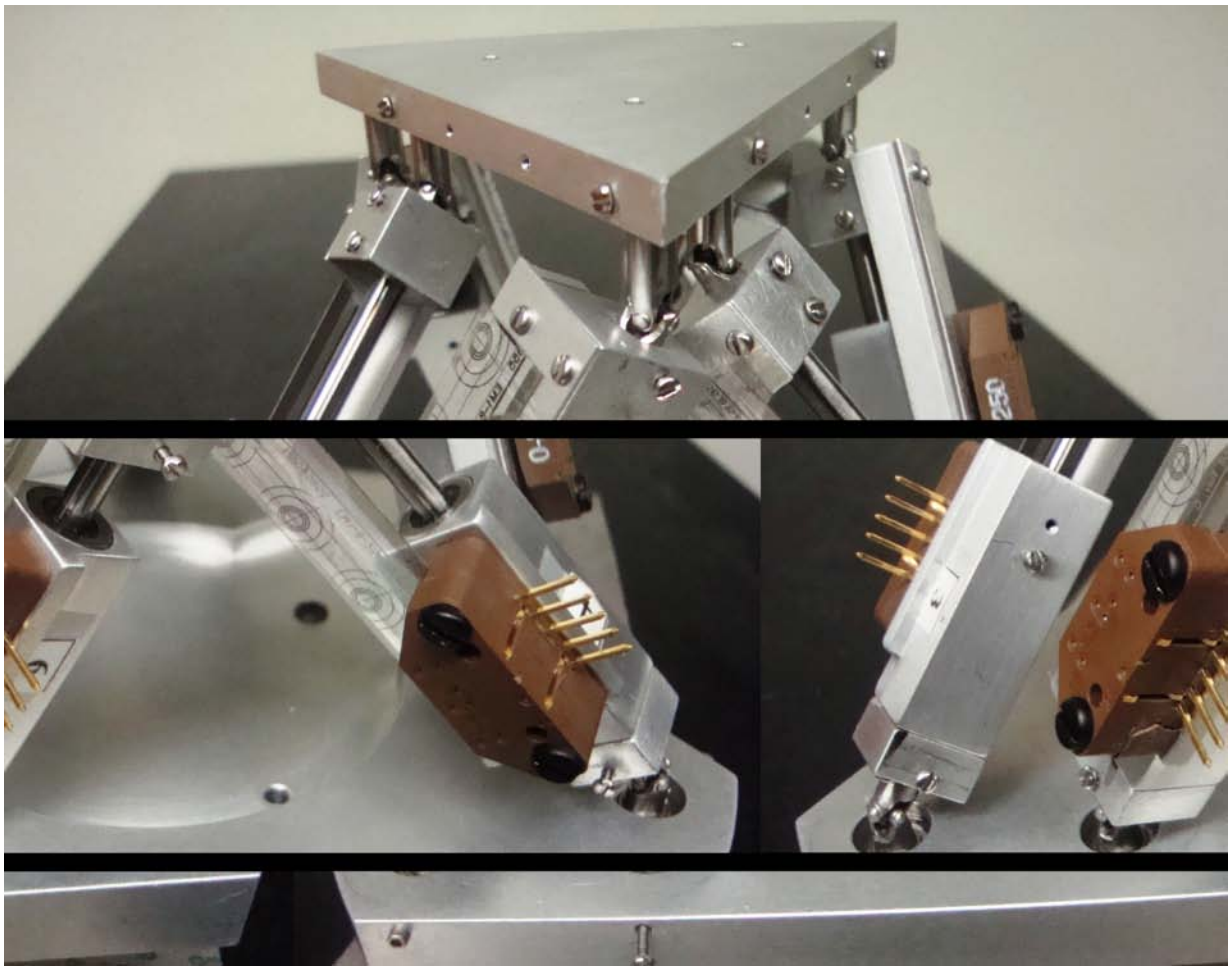

Figure 3-5. Photo of assembled prototype

Figure 3-6. Photo of base and top platform

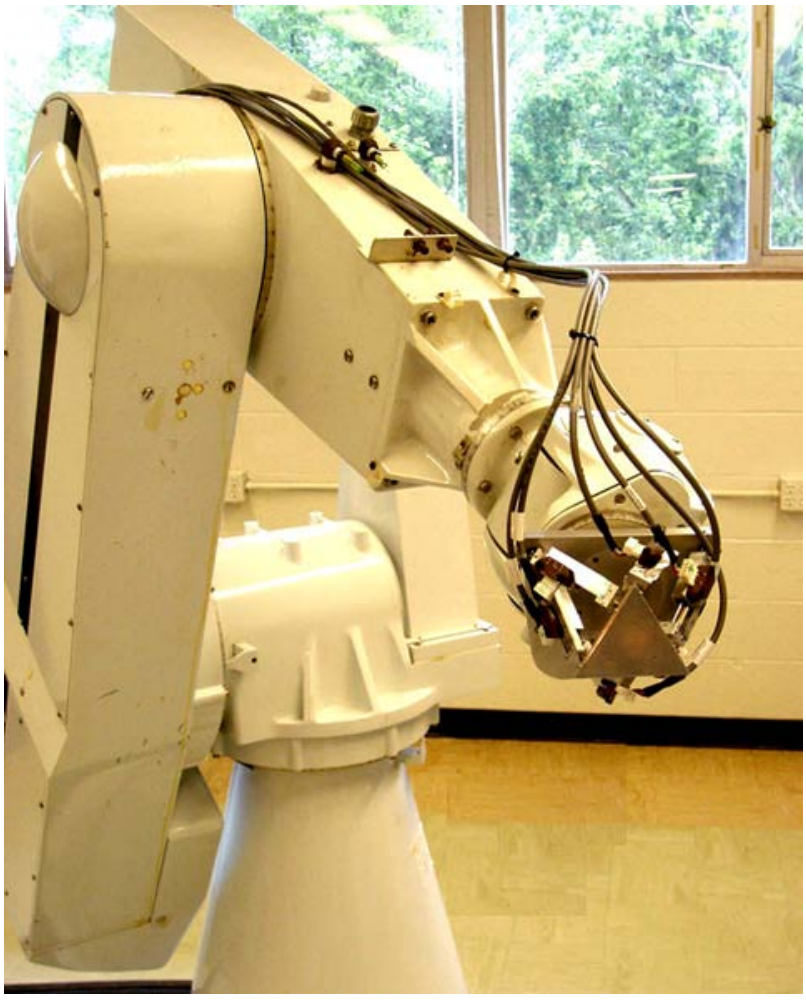

Figure 3-7. The Parallel platform mounted on the distal end of a PUMA industrial robot

CHAPTER 4
ELECTRICAL DESIGN OF THE PARALLEL PLATFORM

In this chapter, the electrical design of the prototype of the force compliant parallel platform is discussed. This involves position sensing with encoders, high speed simultaneous reading of the sensor and sending it to the computer that manages the PUMA industrial robot controller.

4.1 Design Specifications

SP1. The position transducer should have high resolution, accurate.

SP2. The sensed data should be immune to interference due to motion. It needs to be mounted at the distal end of strong industrial manipulator which means it will be subject to high speeds and accelerations.

SP3. The position transducer should be compact

SP4. The position transducer should not add friction to the prismatic joint.

SP5. The position transducer should be fast in sensing and delivering the data.

SP6. The position transducer should ideally give electrical output or some extra transducer needs to be used to convert the output quantity to electrical quantity.

SP7. The data captured from the sensor may need to be sent over long distance i.e. from the distal end of the manipulator to the computer which runs the robot controller.

SP8. The wires (as seen in Figure 3-6) coming from the Parallel platform might get entangled or pulled by the robot during operation, hence its preferable to implement wireless data transfer.

SP9. The data transfer needs to be fast to ensure a sampling rate faster than the rate at which commands are sent to the industrial robot.

SP10. The necessary circuit boards need to be compact

SP11. The circuitry needs to be battery powered.

SP12. The data should be received by the computer using USB interface.

4.2 Position Transducer

Various position transducers were explored. Linear Variable Displacement transducers are big and need AC power. Hence, they were discarded. The next commonly used solution was to use try a potentiometer. Multi-turn rotary potentiometers have much higher resolution over Linear potentiometers but then need some kind of mechanism to convert linear motion into angular motion. Potentiometers are analog sensor and the analog signals are highly susceptible to interference due to vibrations. They would need filtering to get rid of low frequency noise due to vibrations.

Encoders seemed to be the best among all options. They are digital sensor with very high resolution. They can be Optical or Magnetic but Optical one was chosen due to higher resolution and feasibility than magnetic ones. They have been traditionally used for accurate angular position control of joints in serial robot manipulators. Linear encoders are available that are as accurate as commonly used rotary encoders and hence, there is no need for any mechanism to convert linear to angular displacement. Moreover, encoders are non-contact sensor, hence they do not add any friction to the prismatic joint and hence, the compliance of the system doesn't get affected. Encoders are normally incremental type displacement sensors which mean they can sense change in position from a starting point. Error may accumulate with time or the reference point might be lost due to disturbance. Hence, absolute optical encoders were chosen which have an index sensor which demarcates the reference point. Every time an index pulse shows up, the sensor is supposed to zero its position and then start

counting the incremental pulses. Incremental encoding with index can measure change in position but cannot sense direction i.e. increase or decrease in position. Quadrature encoding with index forms the best absolute encoder. It not only can sense direction but also provides 4 times higher resolution than an incremental encoder.

The US Digital EM1 Transmissive Optical Encoders and US Digital LIN Transmissive Linear Strip with 250 counts per inch resolution were chosen. (See Figure 4-1 and 4-2) They are compact, quadrature type and also have index sensing to demarcate the reference point. The EM1 consists of a lensed LED source and a monolithic detector IC enclosed in a small polymer package. It uses phased array detector technology to provide superior performance and greater tolerances over traditional aperture mask type encoders. The resolution of the modules and linear strips must match. Since, these are quadrature encoders 250 stripes per inch on the linear strip can cause 1000 counts per inch of displacement. Hence, the achievable resolution is 0.0254 mm.

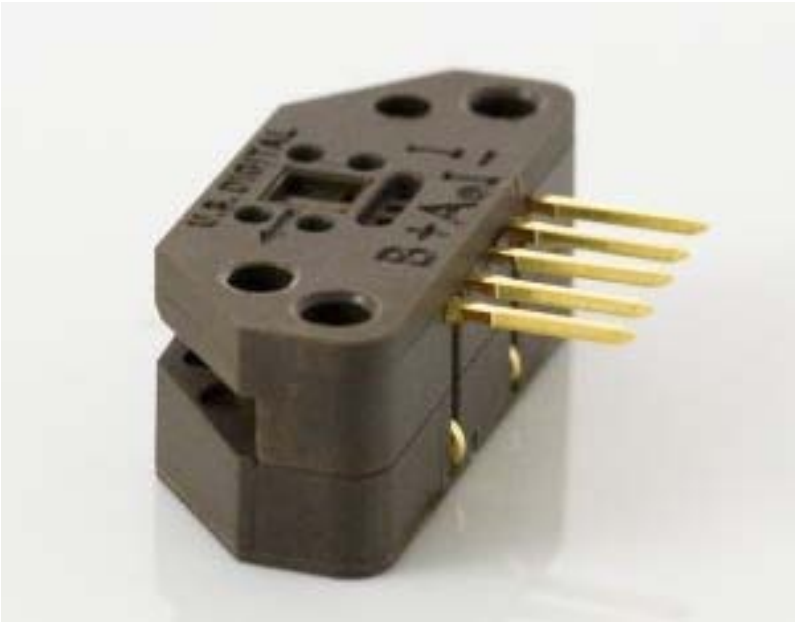

Figure 4-1. US digital EM1 transmissive optical encoder

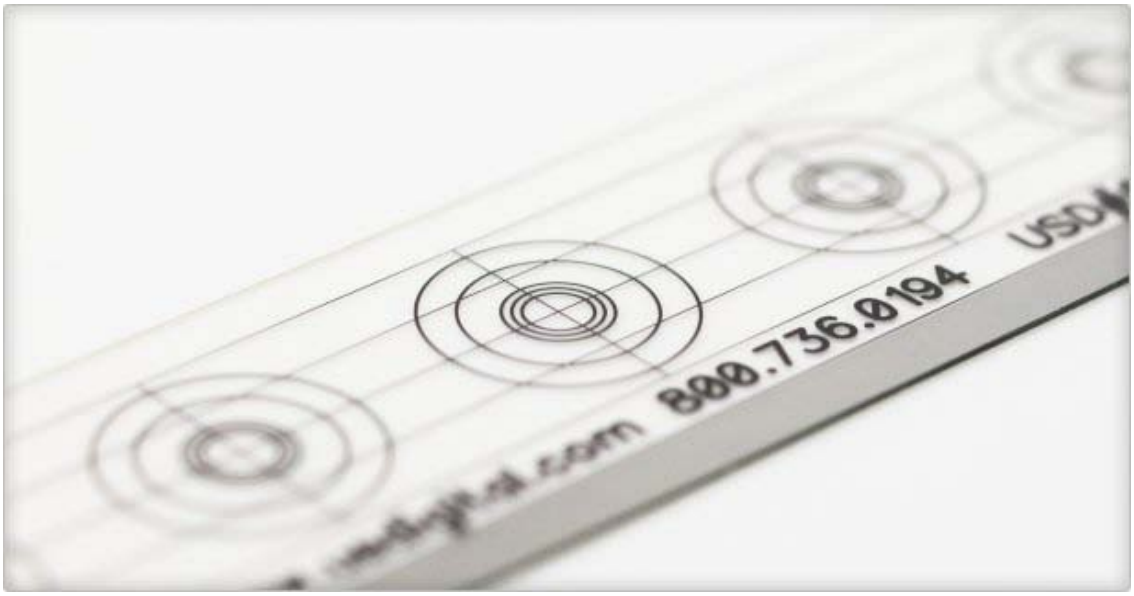

Figure 4-2. US digital LIN transmissive linear strip

4.3 Sensor data Capture

Data from Six Encoders needs to be captured simultaneously. It is difficult to achieve this with a typical microcontroller. Hence, a FPGA was used for the simultaneous data capture. A field-programmable gate array (FPGA) is an integrated circuit designed to be configured by the customer or designer after manufacturing, hence "field-programmable". The FPGA configuration is generally specified using a hardware description language (HDL). FPGAs can be used to implement any logical function. The ability to update the functionality after shipping and the low non-recurring engineering costs relative to an ASIC design offer advantages for many applications. FPGAs contain programmable logic components called "logic blocks" and a hierarchy of reconfigurable interconnects that allow the blocks to be "wired together"—somewhat like a one-chip programmable breadboard. Logic blocks can be configured to perform complex combinational functions, or merely simple logic gates like AND and XOR. In

most FPGAs, the logic blocks also include memory elements, which may be simple flip-flops or more complete blocks of memory.

Figure 4-3. Altera cyclone II EP2C8T144C8

Six parallel running Quadrature decoder digital circuits were configured using the Altera Cyclone II EP2C8T144C8 FPGA running at 25Mhz. Each of them picks up the Quadrature pulses i.e. signals from the two channels A and B coming from the Optical encoders and updates an 8 bit counter which gets incremented or decrementing based on direction of displacements. Since the leg connectors are supposed to move only by as small as $\pm$ 5mm, 8 bit counters were deemed sufficient. This also ensured a smaller sensor data packet size and consequent faster Sampling Rate.

Quadrature encoding uses two channels - A and B. The two signals A and B can either be HIGH or LOW. For any change in state on the signals A and B, the current new state is compared with the previous state and based on the Transition table shown in Figure 4-4, a counter is either incremented or decremented. Increment can be used for positive direction of displacement and decrement can be used for negative direction of displacement of vice-versa.

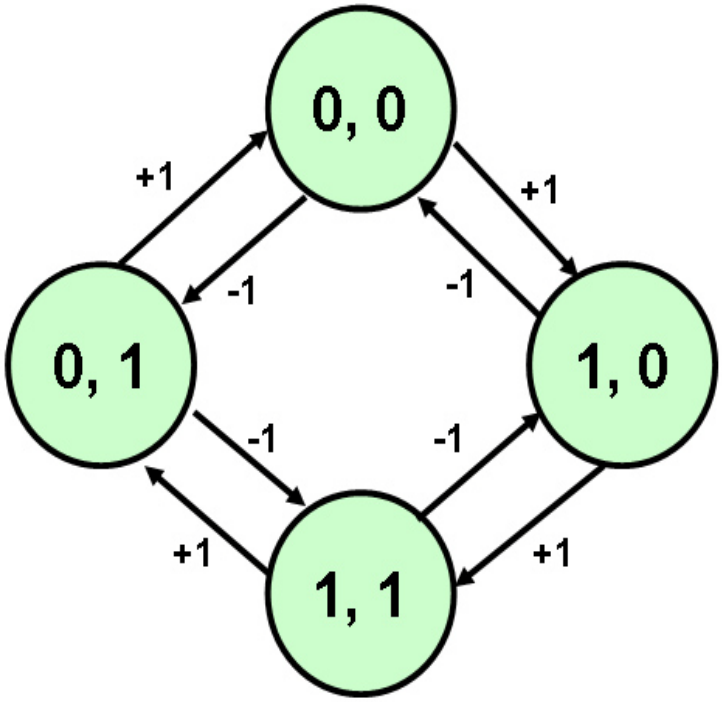

Figure 4-4. Quadrature encoder state transition diagram. (The values inside the circle indicate HIGH and LOW state on Channel A and Channel B while values on the arrows indicate increment or decrement of counter)

The above explained Quadrature encoding scheme is decoded using a Quadrature decoder. It can be implemented in various ways. It can be done using a simple hardware circuit as shown in Figure 4-5. This circuit is sometimes called a "4x decoder" because it counts all the transitions of the quadrature inputs. This improves the resolution by 4 times compared to incremental encoding which give just one signal.

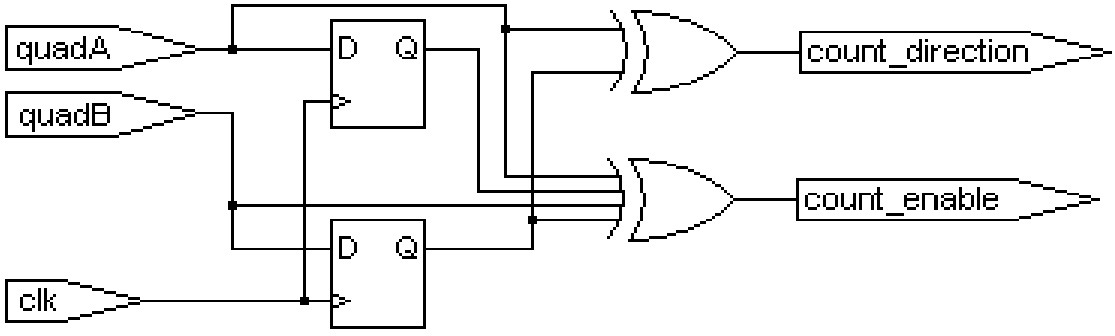

Figure 4-5. Quadrature decoder digital circuit

Figure 4-5 assumes that the two Quadrature channel signals were synchronous to the clock which is mostly not the case. But, introducing 2 extra D-flipflops per input channel solves the issue. (Figure 4-6) [11]

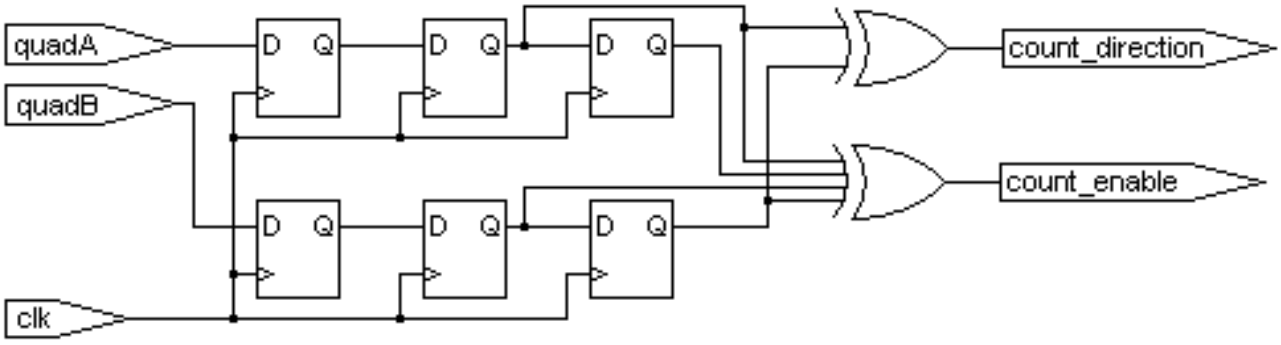

Figure 4-6. Practical quadrature decoder digital circuit

The index pulse is the third input signal which appears only when the sensor is right over a particular point on the linear transmissive strip. This resets the counter to a hard coded value corresponding to the home or reference position. This ensures absolute encoding. The VHDL code and block design is given in Appendix C.

4.4 Data Transmission

Multiplexed parallel data lines are used to read each 8 bit register holding the instantaneous counter value corresponding to each connector leg. This is done by an Atmel Atmega128 micro controller running at 16 mhz. The micro controller then forms and sends out packets of sensor data in asynchronous serial format to an Xbee wireless module at Baud rate of 115200. The 30 bytes ASCII packet structure of the sample data is given in Table 4-1.

The checksum byte is used to check data integrity. The receiver finds the checksum of received bytes and compares with this checksum number at the end of the data packet to check if the data received is same as what was sent by the transmitter.

This ensures more robust communication, if the data received doesn't match with the data sent then that particular packet is rejected as erroneous.

Table 4-1. Sensor data packet structure

Byte Position	ASCII Character (One Byte)	Description
1	$	Header byte
2	A	Shows that the next three bytes represent count for Encoder A
3	X-100	Counter Value of Encoder A
4	X-10	Three digit decimal number (000 - 256) converted as it is
5	X-1	to ASCII characters. Ex – $(225)_{10}$ => '2' '2' '5' ASCII
6	B	Shows that the next three bytes represent count for Encoder B
7	X-100	Counter Value of Encoder B
8	X-10	Three digit decimal number (000 - 256) converted as it is
9	X-1	to ASCII characters. Ex – $(225)_{10}$ => '2' '2' '5' ASCII
10	C	Shows that the next three bytes represent count for Encoder C
11	X-100	Counter Value of Encoder C
12	X-10	Three digit decimal number (000 - 256) converted as it is
13	X-1	to ASCII characters. Ex – $(225)_{10}$ => '2' '2' '5' ASCII
14	D	Shows that the next three bytes represent count for Encoder D
15	X-100	Counter Value of Encoder D
16	X-10	Three digit decimal number (000 - 256) converted as it is
17	X-1	to ASCII characters. Ex – $(225)_{10}$ => '2' '2' '5' ASCII
18	E	Shows that the next three bytes represent count for Encoder E
19	X-100	Counter Value of Encoder E
20	X-10	Three digit decimal number (000 - 256) converted as it is
21	X-1	to ASCII characters. Ex – $(225)_{10}$ => '2' '2' '5' ASCII
22	F	Shows that the next three bytes represent count for Encoder F
23	X-100	Counter Value of Encoder F
24	X-10	Three digit decimal number (000 - 256) converted as it is
25	X-1	to ASCII characters. Ex – $(225)_{10}$ => '2' '2' '5' ASCII
26	*	Trailer byte
27	Y-16	Checksum = computed by doing a XOR of all the bytes
28	Y-1	between the header and trailer bytes. The result is one byte which can be represented as two digit Hexadecimal number. (00- FF). It is converted as it is into ASCII characters. Ex – $(A4)_{16}$ => 'A' '4' ASCII
29, 30	CR	Carriage Return or '\n' – demarcates end of packet

The system is capable of sending out one full packet i.e. one sample in 4ms (time is counted from the point of asking to point of receiving) i.e. maximum sampling rate can be 250 Hz. The micro controller ensures both continuous mode as well as polled mode of data extraction. The selection between the modes is interrupt driven. If the micro controller receives an ASCII character ‘C’ or ‘c’, it starts sending out data in continuous mode as a 100 Hz sampling rate. But if the micro controller receives an ASCII character ‘P’ or ‘p’, it responds by sending out 1 packet of data or one sample and then stops sending. Any other ASCII character sent to the micro controller will have no effect on the data transmission state.

Since these days most computers don’t have the typical DB-9 serial port, data transmission to a computer was tried using USB. Serial TTL level signals can be easily converted to send to USB port using FTDI USB transceivers. The FT232 USB UART IC was tried. This can be interfaced by any high level language program running on Windows based Computer with a USB port and installed FTDI USB driver. FTDI offers two USB drivers – VCP and DTXX. VCP stands for virtual COM port which means when this is used, the USB port will appear as a traditional serial COM port to the computer program and traditional serial capture programs written in high level languages can be used. The traditional Serial COM ports on a computer are directly connected to the mother board and interrupt driven. Hence, when a character is transmitted or received the CPU would be interrupted and go to a routine to handle the data. This meant that a user could be reasonably certain that, given a particular baud rate and data rate, the transfer of data could be achieved without any real need for flow control. The hardware interrupt ensured that the request would get serviced. Therefore data could be

transferred without using handshaking and still arrive into the PC without data loss. USB does not transfer data using interrupts. It uses a scheduled system and as a result, there can be periods when the USB request does not get scheduled. [5]

The sensor capable of sending out data at 4 ms sampling time when connected to a computer directly using the FTDI USB transceiver showed disastrous results, the sampling time was not consistent and varied between 30-60 ms. Best throughput through USB can be ensured by any of these three solutions. [5]

1. The value of latency timer and value buffer size of the FTDI chip must match the sampling rate and data packet size
2. An event character can be enabled i.e. if the event character is enabled and it is detected in the data stream, then the contents of the device buffer are sent immediately.
3. Hardware Handshaking i.e. level on one of the RS232 status lines needs to be changed to cause the contents of the device buffer to be sent immediately.

Solution 2) was used as it was most easy to implement using Software method. It needs the D2XX drivers for the USB transceiver. D2XX drivers allow direct access to the USB device through a DLL. Application software can access the USB device through a series of DLL function calls. Not only are these drivers more powerful then the VCP in improving the throughput but they are also not dependant on COM port number. While using VCP, the COM port number of the port connected to a device needs to be hard coded in the high level program. When a USB device using FTDI transceiver is connected to a computer, a randomly generated COM port number is assigned to it. Using VCP would need the programmer or user to go into Device manager and find out the COM port number and provide it to the program. On the other hand, using D2XX driver lets the program choose a USB device based on its unique Serial number or Device description hard coded in the EEPROM of each FTDI USB transceiver. Hence,

this ensures that a particular USB device connected to any computer running the program will automatically find the USB device. Due all these merits, the D2XX driver and its DLL function calls were used. [6] The event character '\n' was set on the USB transceiver chip using software function calls. Since '\n' or Carriage Return demarcates the end of the data packet, this ensured that all the data received by the USB buffer be sent to the computer as soon as this character is encountered. This successfully resolved the USB bottleneck problem and reduced the sampling time to 4 ms when connected directly without the wireless link.

The next bottle neck is the Wireless link. Xbee or also known as Zigbee can make a serial line wireless i.e. if two devices are communicating over asynchronous serial then the wired connection can be easily replaced by two Xbee modules one on each end as shown in Figure 4-5. But, the best achievable sampling time increased from 4ms to 16ms. Hence, the maximum cycle time of the current system with wireless capability is 62.5Hz.

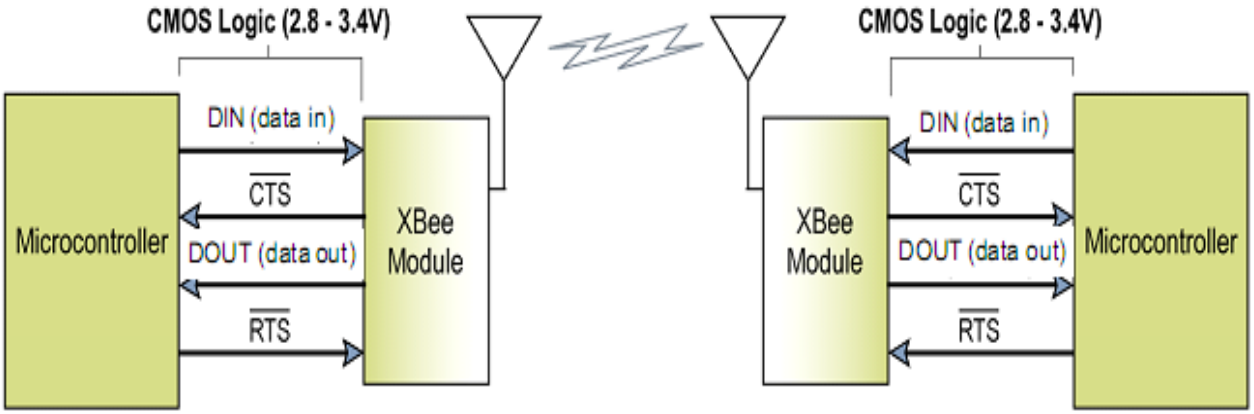

Figure 4-7. Two Xbee modules can replace a serial communication line

CHAPTER 5
RESULTS AND CONCLUSION

In this chapter, the individual components of the designed manipulator are tested to validate the machine design and theoretical analysis presented in the previous Chapters 1 through 4. In order to calibrate each leg's stiffness, first the force sensor is calibrated. An optical encoder measures the compliant displacement of the leg and the load cell records the applied force. The force-displacement relationship is provided for each leg and the results are analyzed. The parallel platform is then assembled for the 6 DOF wrench measuring testing. Several experiments are presented and the results are analyzed. At the end of this chapter, a summary of the work is followed by conclusions and future work suggestions.

5.1 Calibration Experiment for the Force Sensor

A load cell was used to measure the axial force applied on the individual leg. The rated capacity of the load cell was 5 lb, (22.246 N) and the output of the load cell was an analog voltage signal, ranging from -5~+5 Vdc. The rated output is 2mV/V± 20%. It was necessary to calibrate the load cell first to ensure the validity and accuracy of the experiments' results. The load cell output analog signal is connected to an A/D port of a multi-functional I/O board and the value of the voltage is recorded with the corresponding known force, which is provided by a set of standard weights for accurate force calibration. The mapping of the force/voltage relationship is shown in Figure 5-2 and Figure 5-3. Five additional sets of experimental data were analyzed and the plots are very similar, so only one plot is shown here.

5.2 Individual Leg Calibration Experiment

After calibrating the load cell, it is necessary to calibrate the compliant connectors and identify the stiffness property for each of them. During the experiment, the compliant connector is fixed vertically and is attached to the load cell in such a way that the applied external force causing either elongation or compression can be detected properly. The physical quantities, force and displacement, are detected by the load cell and the optical encoder.

The Optical encoder returns counts. A mapping relationship was experimentally determined to find $\Delta l = l - l_0$ i.e. the corresponding change of length from free length. The mapping graph for each leg is given in Figures 5-4 through 5-9.

Table 5-1. Extension Vs Encoder count relationship

Leg number	Extension(inches) vs. Encoder count linear relationship	Encoder counts for index	Encoder counts for relaxed state
Leg 1	y = - 0.000993 x + 0.068673	100	69
Leg 2	y = - 0.00099 x + 0.06135	100	65
Leg 3	y = - 0.00101 x + 0.0751	100	79
Leg 4	y = - 0.00122 x + 0.1364	100	120
Leg 5	y = - 0.00100 x + 0.076	160	75
Leg 6	y = - 0.00095 x + 0.06465	100	87

The optical encoder is attached on the compliant leg both for the calibration experiment and for the designed operation. Axial force is applied on the top of the compliant leg with variable magnitude and direction in order to get the stiffness mapping of the leg for both compression and elongation. The resolution of the optical encoder is 1000 counts/inch. The individual plot of the stiffness mapping for each of the six leg connectors is shown in 5-10 through 5-15.

In the calibration plots, the displacement is measured in mm and force measured in Newtons. In the original data file, the displacement at each sample time is recorded as encoder counts and the force is recorded as digitized voltage value. .

Then the units are converted by the load cell calibration experiment results together with the following conversion Equation 3-3:

$$1\,in = 25.4\,mm$$
$$1\,lb = 453.6\,gram = 4.448\,N \tag{3-3}$$

Then, the data in the plots is used to build six individual look-up tables of displacement vs. force for each leg. During operation, the relative displacement is measured and the corresponding force value is obtained from the look-up table. These calibration tables can also be replaced by linear regression of the data for less-accurate operations, and thus a “linear spring constant” is assigned to each leg.

Table 5-2. Spring constants

Leg number	Spring constants (N/mm)
Leg 1	3.0914
Leg 2	3.0469
Leg 3	3.1003
Leg 4	3.1047
Leg 5	2.9757
Leg 6	3.038

5.3 Repeatability

The Top platform was displaced from the stable (Zero Wrench) state and left to come back to its stable state. This was done multiple times and every time after device comes back to stable state, the Encoder counts and corresponding leg lengths were noted. The readings give an idea of the repeatability of the device i.e. how good the measured length readings are when the leg lengths come back to the actual same values. From Table 5-3, we can see that the repeatability error is negligible.

Table 5-3. Repeatability test – Observe the change in Encoder counts and Extension (in mil; 1mil = 0.001 inches)

Leg	Relaxed state of the legs	Stable state readings 1	Stable state readings 2	Stable state readings 3	Stable state readings 4
Leg 1	69 = 0 mil	80 = - 11mil	78 = - 9 mil	76 = - 7 mil	78 = - 9 mil
Leg 2	65 = - 3 mil	60 = 2 mil	61 = 1 mil	62 = - 0 mil	61 = 1 mil
Leg 3	79 = - 5 mil	76 = - 2 mil	79 = - 5 mil	79 = - 5 mil	78 = - 4 mil
Leg 4	120 = - 10 mil	112 = 0 mil	127 = - 18mil	133 = - 26 mil	123 = - 14 mil
Leg 5	75 = 1 mil	89 = - 13 mil	89 = - 13 mil	86 = - 1 mil	86 = - 10 mil
Leg 6	87 = 18 mil	96 = - 26 mil	93 = - 23.7 mil	94 = - 24.6 mil	93 = - 23.7 mil

5.4 Forward Kinematic Analysis and Theoretical Compliance Matrix

The geometric properties were hard coded in a high level program written to do the forward kinematic analysis for the prototype. It takes instantaneous leg lengths as inputs and finds the position and orientation of top mobile platform relative to the fixed base platform. To find the position and orientation, coordinate systems are defined on the top and base platform as shown in Figure 5-1. A transformation matrix is calculated that defines the position and orientation between two coordinate systems. [2]

Table 5-4. Test case: Input leg lengths

Leg Number	Leg 1	Leg 2	Leg 3	Leg 4	Leg 5	Leg 6
Leg Lengths (mm)	80.1054	68.2032	80.8928	67.9492	80.8928	66.8570

Result of Forward analysis gives 4 Transformation matrices between Coordinate systems 0 and 1. The one in which z-axis remains most similar to chosen z-axis is used.

$$ {}^{base}_{Top}T = {}^{0}_{1}T = \begin{bmatrix} 0.5017 & 0.8647 & -0.0243 & 30.1091 \\ -0.8647 & 0.5021 & 0.0154 & 51.6518 \\ 0.0256 & 0.0133 & 0.9996 & 58.5839 \\ 0.0000 & 0.0000 & 0.0000 & 1.0000 \end{bmatrix} \quad (3\text{-}4) $$

where the units of the first three columns are dimensionless and the units of the top three terms of the fourth columns are in millimeters.

The theoretical compliance matrix corresponding to the position of the top platform as defined by ${}^{0}_{1}\mathbf{T}$ (from Equation 3-4) was calculated using Equation 2-13 using the geometric properties and spring values for the fabricated device. The calculated matrix is found to be

$$[\mathbf{K}]_{\text{theor}} = \begin{bmatrix} 3.0505 & 0.0426 & -0.0239 & -21.406 & 211.79 & -101.96 \\ 0.0426 & 3.0365 & 0.0265 & -205.78 & -21.241 & 180.95 \\ -0.024 & 0.0265 & 12.101 & 412.15 & -732.38 & 42.647 \\ -21.406 & -210.72 & 411.97 & 33777 & -24895 & -10396 \\ 216.73 & -21.241 & -732.36 & -24898 & 64519 & -11169 \\ -101.78 & 180.93 & 42.647 & -10226 & -10906 & 18475 \end{bmatrix} \tag{5}$$

where the terms of the upper left 3×3 sub matrix have units of N/mm, the terms of the upper right and lower left 3×3 sub matrices have units of N, and where the terms of the lower right 3×3 sub matrix have units of N mm.

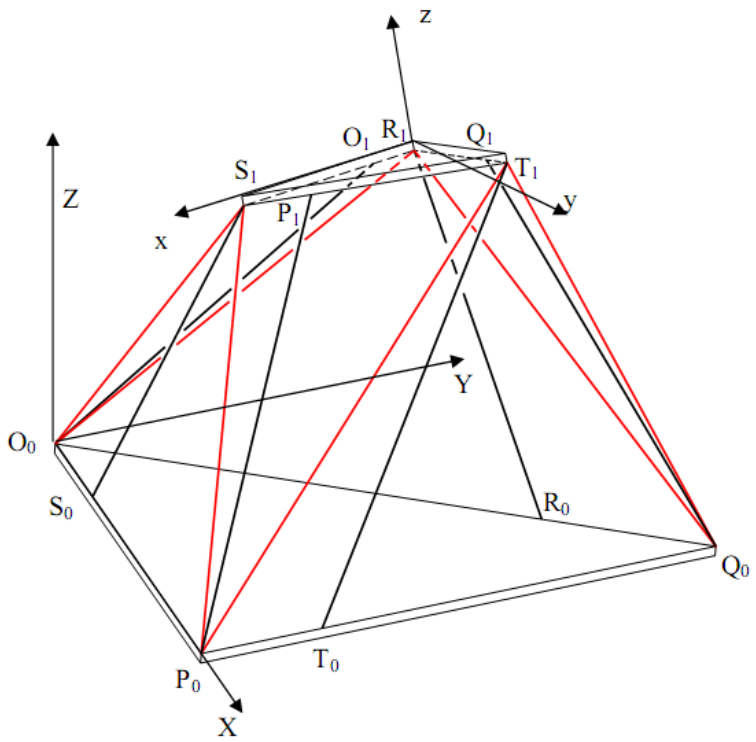

Figure 5-1. Coordinate systems 0 and 1 fixed in the base and top platform respectively

5.5 Conclusion

This work will allow for an implementation of the Theory of Kinestatic Control where a spatial serial manipulator can be commanded to move the base platform in order to change the wrench experienced at the top platform. The system's stiffness will be dependant on the configuration of the robot system which includes the serial industrial robot, passive parallel platform and the gripper or tool. The ability to accurately modeling the system stiffness will decide the control performance for displacement and force.

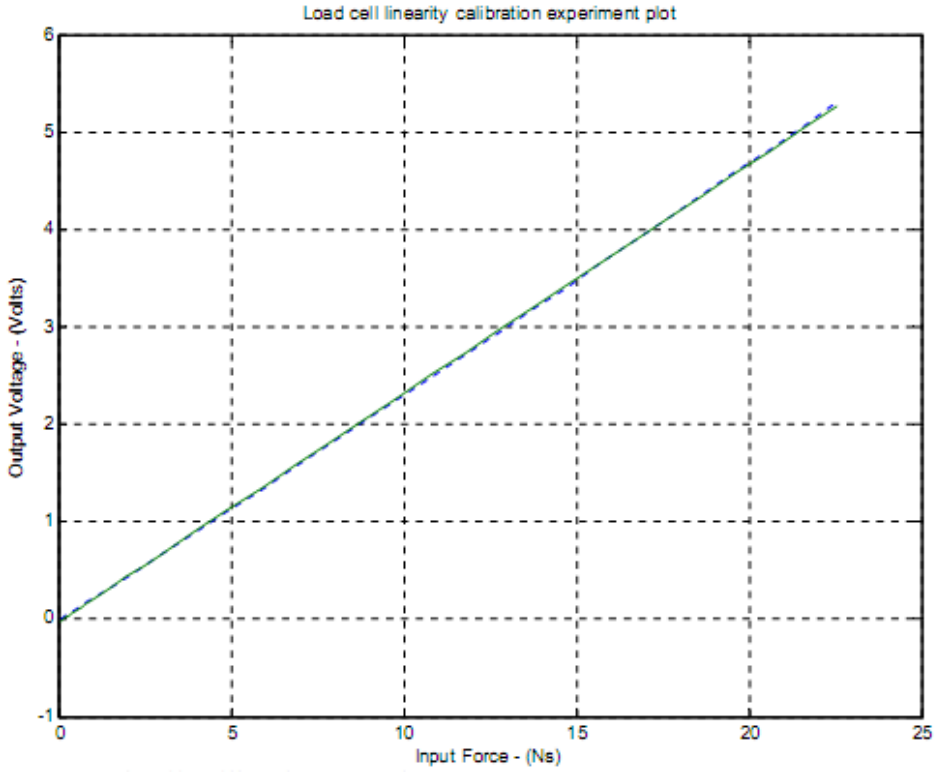

Figure 5-2. Load cell calibration experiment

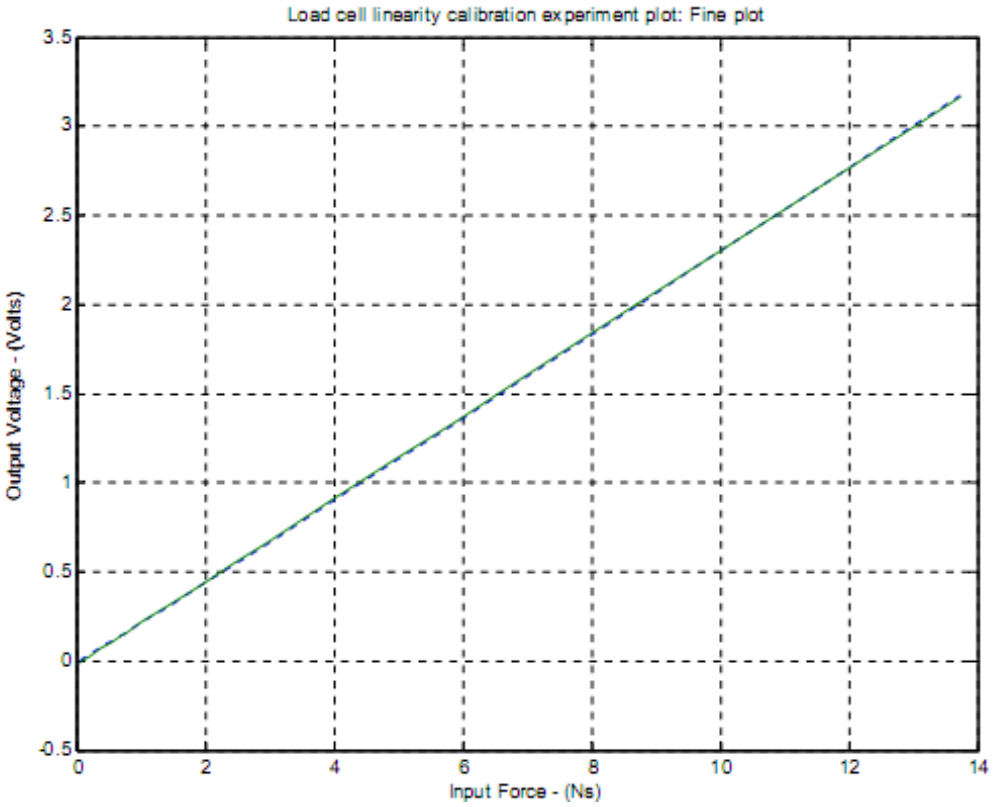

Figure 5-3. Load cell calibration experiment - opposite direction

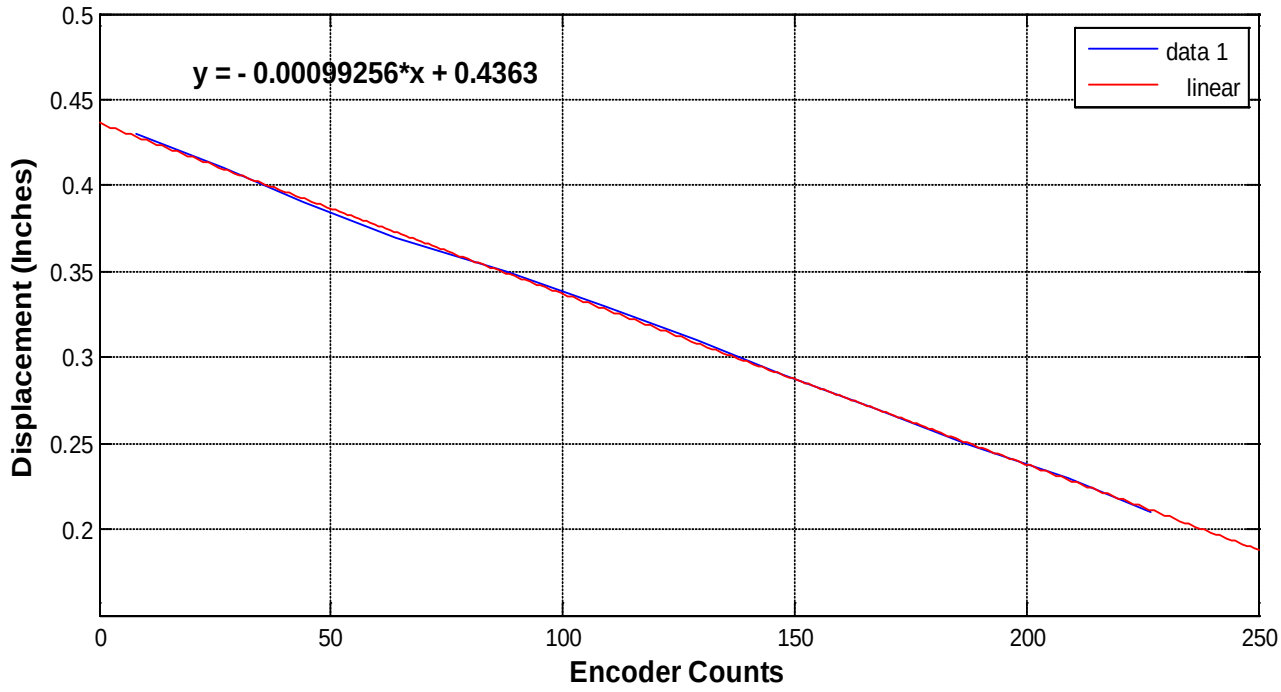

Figure 5-4. Linear Curve fit of displacement vs. encoder counts for encoder 1

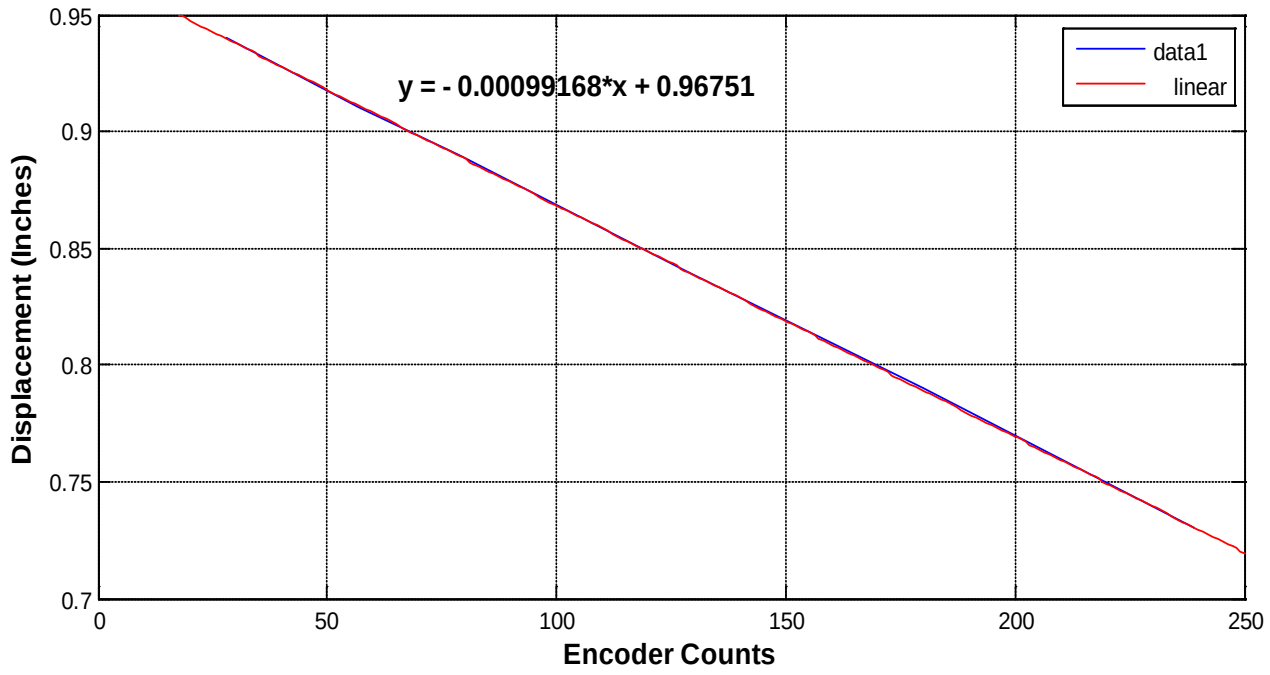

Figure 5-5. Linear curve fit of displacement vs. encoder counts for encoder 2

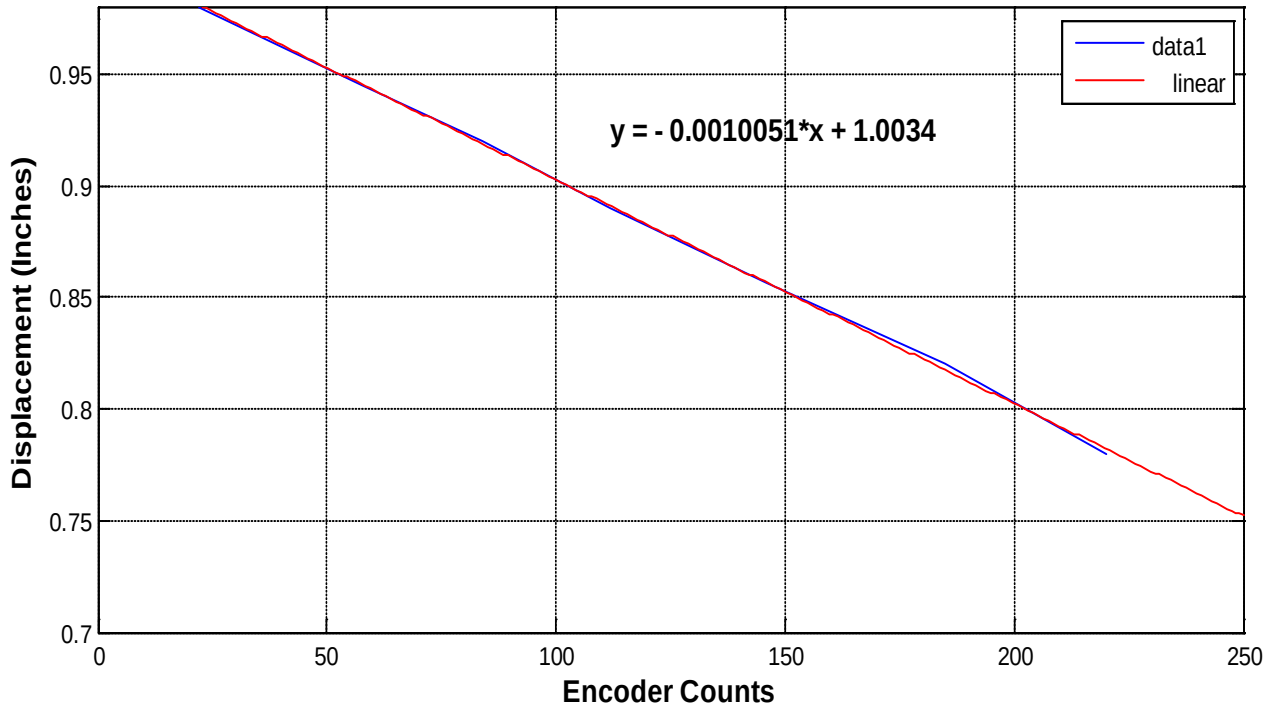

Figure 5-6. Linear curve fit of displacement vs. encoder counts for encoder 3

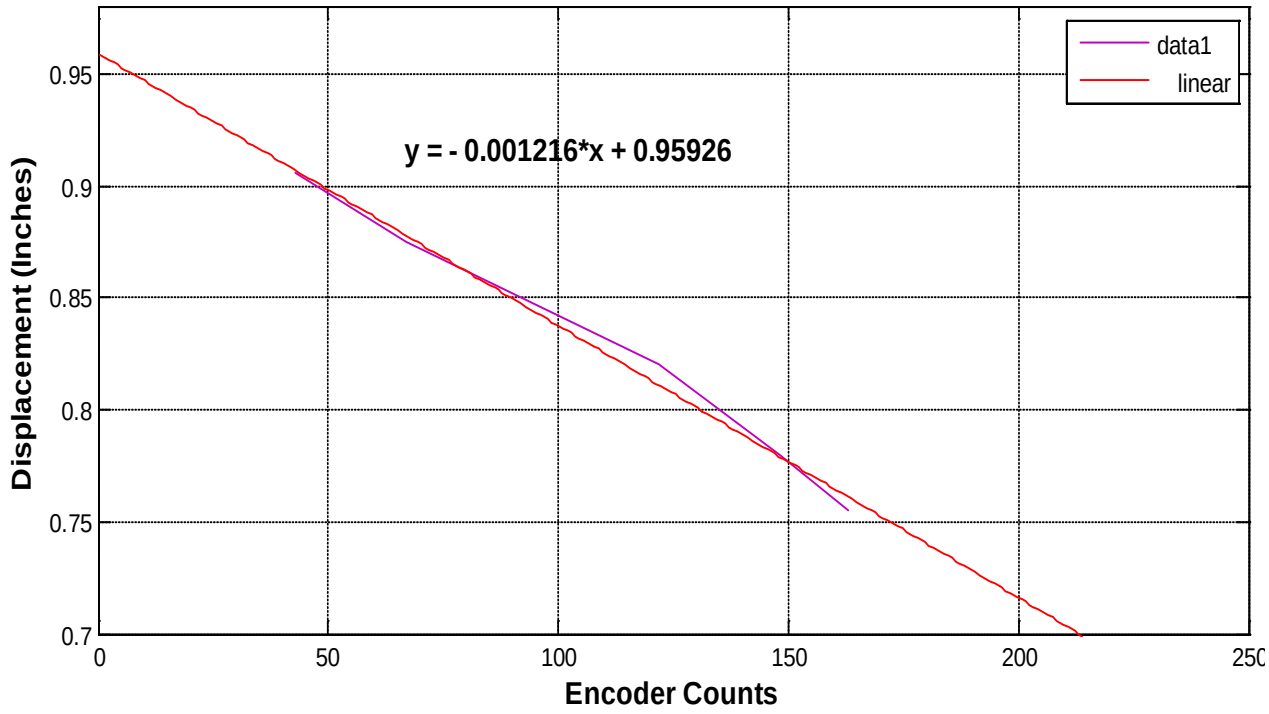

Figure 5-7. Linear curve fit of displacement vs. encoder counts for encoder 4

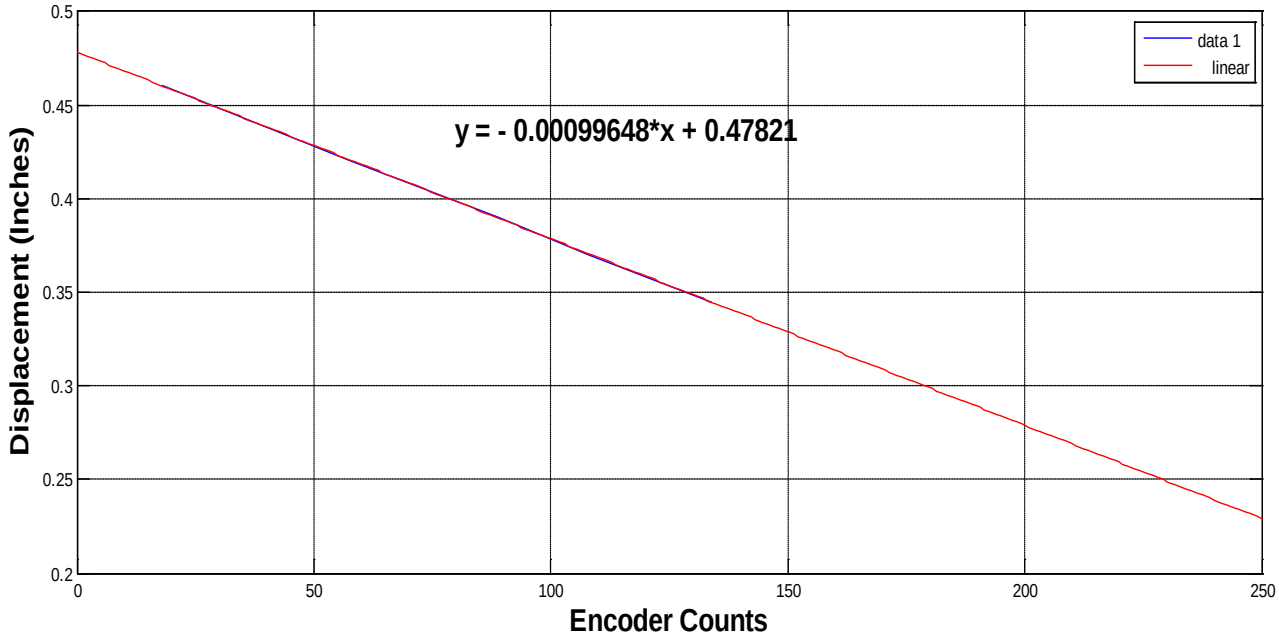

Figure 5-8. Linear curve fit of displacement vs. encoder counts for encoder 5

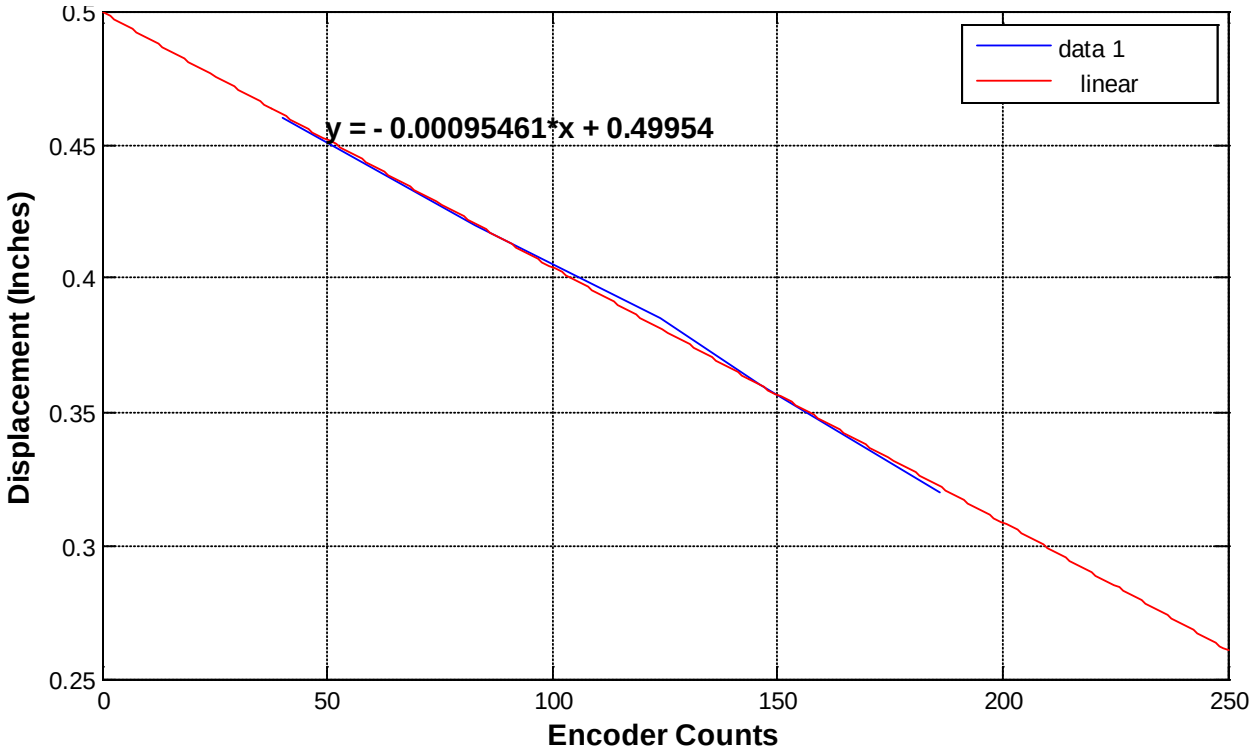

Figure 5-9. Linear curve fit of displacement vs. encoder counts for encoder 6

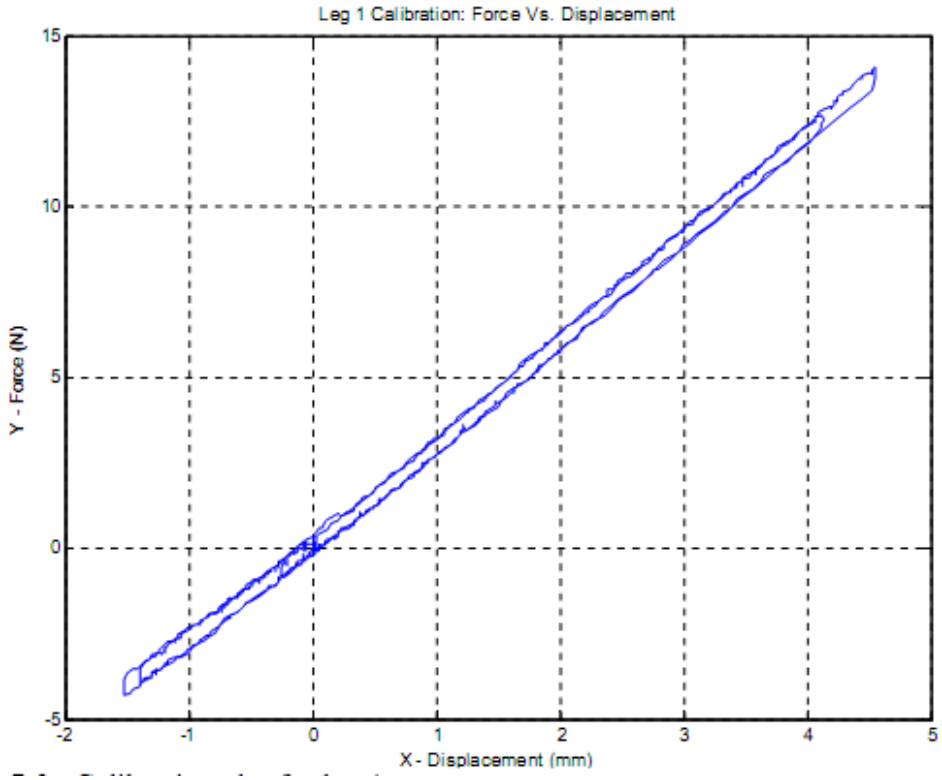

Figure 5-10. Calibration plot for leg-1

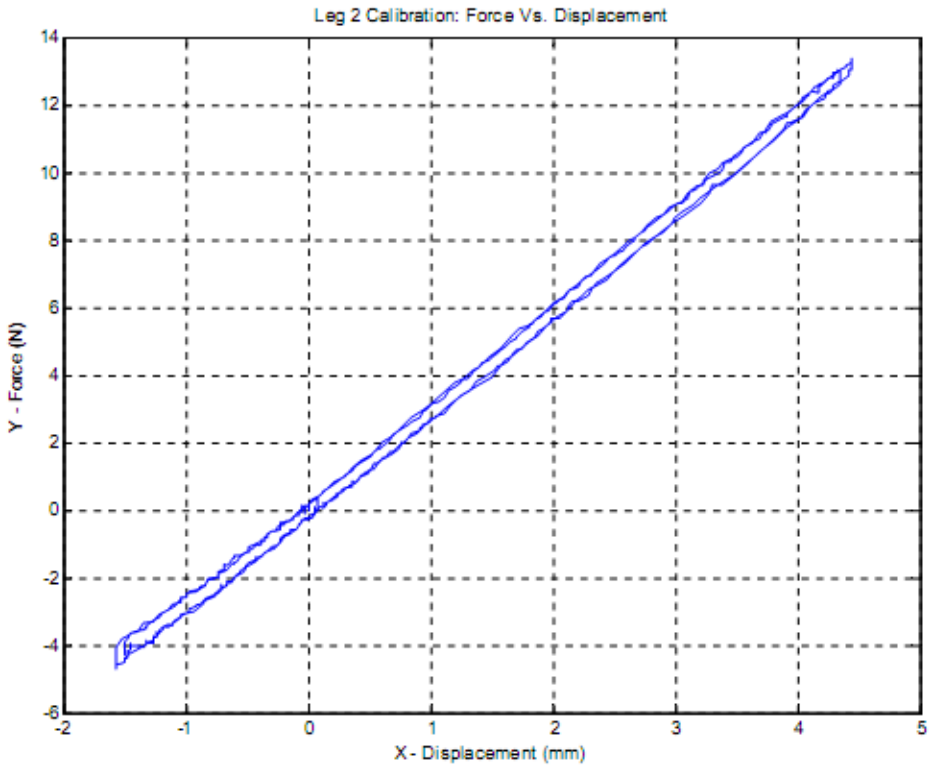

Figure 5-11. Calibration plot for leg-2

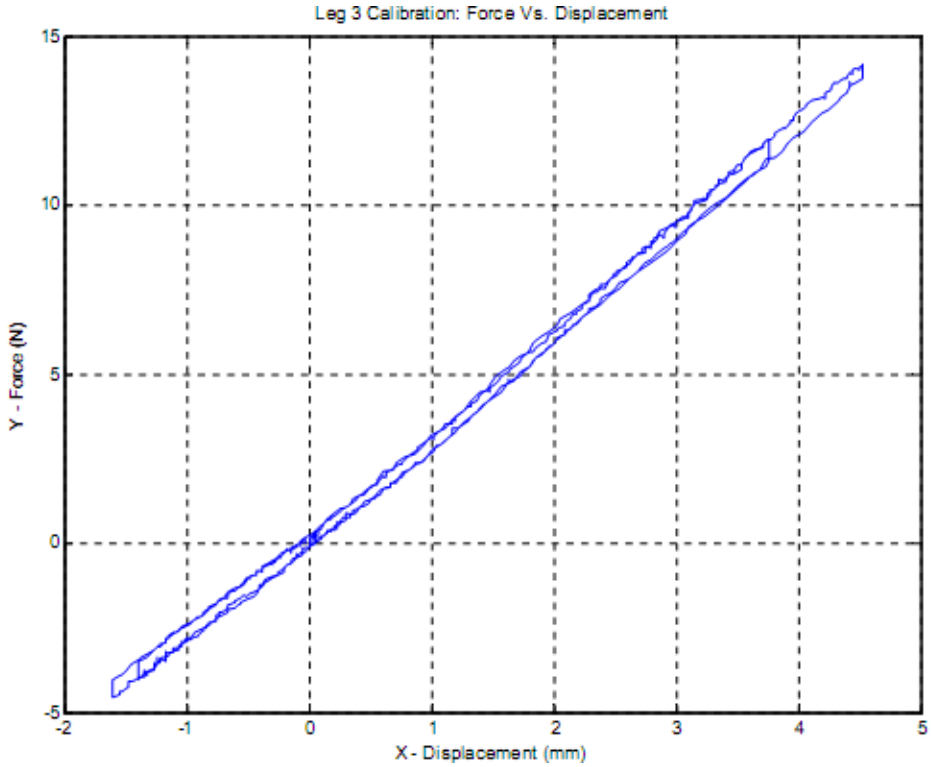

Figure 5-12. Calibration plot for leg-3

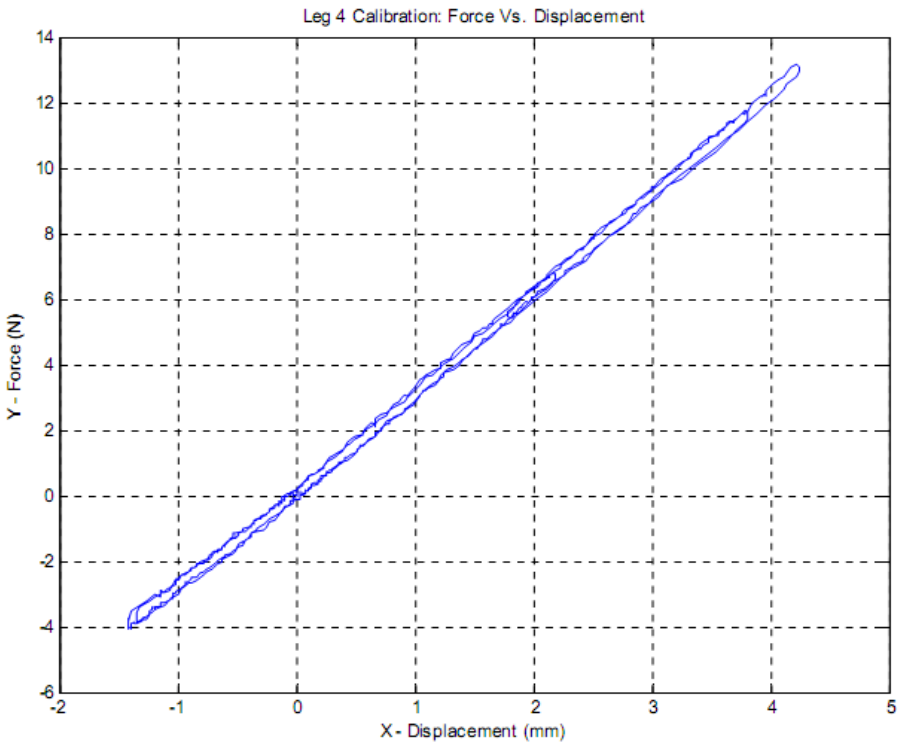

Figure 5-13. Calibration plot for leg-4

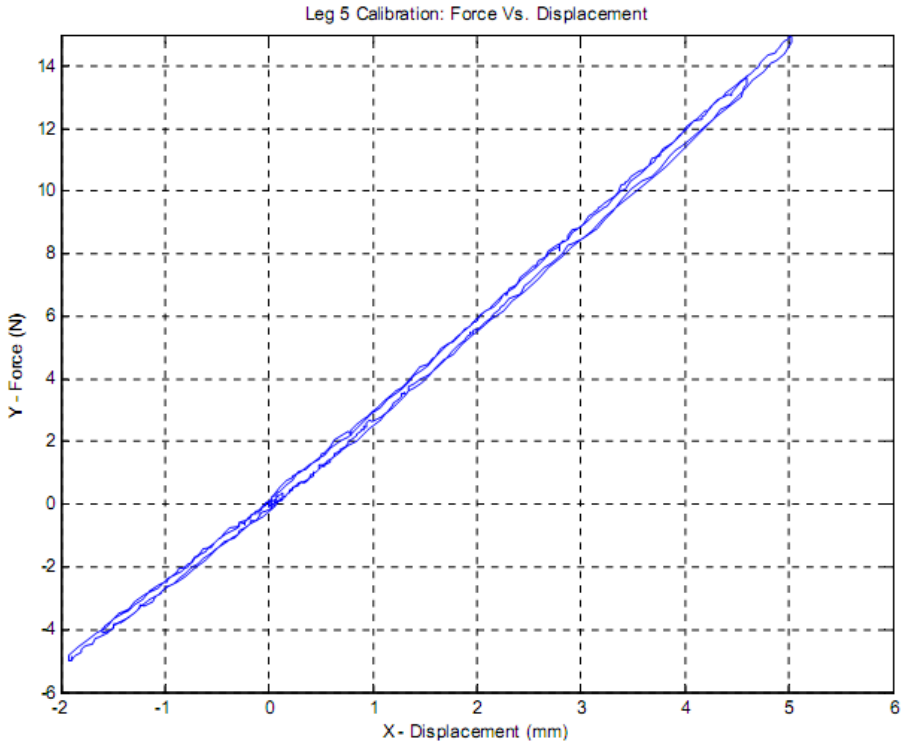

Figure 5-14. Calibration plot for leg-5

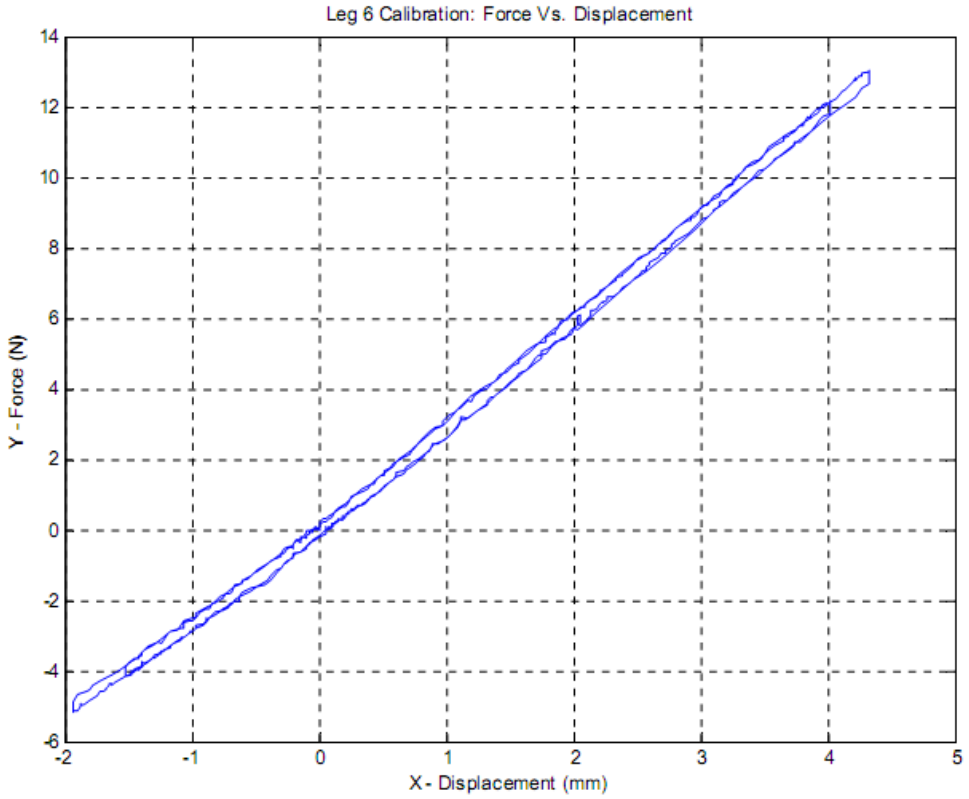

Figure 5-15. Calibration plot for leg-6

APPENDIX A
COORDINATES OF POINT

The position vector to a point Q_1 from origin O is given by $\mathbf{r_1}$ and can be expressed in the form

$$\mathbf{r_1} = \frac{x_1\mathbf{i} + y_1\mathbf{j} + z_1\mathbf{k}}{w_1} \tag{A-1}$$

Where x_1, y_1, z_1 have units of length and w_1 is dimensionless and they form the homogenous coordinates of point Q_1 as (w_1, x_1, y_1, z_1). [1]

APPENDIX B
COORDINATES OF LINE

The join of two distinct points $\mathbf{r}_1$ and $\mathbf{r}_2$ determine a line. The vector $\mathbf{S}$ whose direction is along the line may be written as

$$\mathbf{S} = \mathbf{r}_2 - \mathbf{r}_1 \tag{B-1}$$

Direction is a unit less concept and thus, the elements of vector $\mathbf{S}$ are dimensionless. The vector $\mathbf{S}$ may be alternatively expressed as

$$\mathbf{S} = L\mathbf{i} + M\mathbf{j} + N\mathbf{k} \tag{B-2}$$

where $L = x_2 - x_1$, $M = y_2 - y_1$ and $N = z_2 - z_1$ are defined as the dimensionless direction ratios. They are related to $|\mathbf{S}|$ by

$$L^2 + M^2 + N^2 = |\mathbf{S}|^2 \tag{B-3}$$

For $|\mathbf{S}| = 1$, Equation (B-3) reduces to

$$L^2 + M^2 + N^2 = 1$$

If $\mathbf{r}$ designates a vector from the origin of the coordinate system to any general point on the line, then it's apparent that the vector $\mathbf{r} - \mathbf{r}_1$ is parallel to $\mathbf{S}$. Thus it may be written that,

$$(\mathbf{r} - \mathbf{r}_1) \times \mathbf{S} = 0 \tag{B-4}$$

This can be expressed in the form

$$\mathbf{r} \times \mathbf{S} = \mathbf{S}_{0\mathbf{L}} \tag{B-5}$$

Where

$$\mathbf{S}_{0\mathbf{L}} = \mathbf{r}_1 \times \mathbf{S} \tag{B-6}$$

is the moment of the line about origin and is clearly origin dependant. The elements of vector $\mathbf{S_{OL}}$ have units of length. Furthermore, since $\mathbf{S}_{0\mathbf{L}} = \mathbf{r_1} \times \mathbf{S}$ the vectors $\mathbf{S}$ and $\mathbf{S}_{0\mathbf{L}}$ are perpendicular and must satisfy the orthogonality condition.

$$\mathbf{S} \cdot \mathbf{S}_{0\mathbf{L}} = 0 \tag{B-7}$$

The coordinates of the line will be written as $\{\mathbf{S}; \mathbf{S}_{0\mathbf{L}}\}$ and will be referred to as the Plücker coordinates of the line. The semi-colon is introduced to signify the dimensions of $|\mathbf{S}|$ and $|\mathbf{S}_{0\mathbf{L}}|$ are different. The coordinates $\{\mathbf{S}; \mathbf{S}_{0\mathbf{L}}\}$ are homogenous since from (B-5) the coordinates $\{\lambda\mathbf{S}; \lambda\mathbf{S}_{0\mathbf{L}}\}$ where λ is a non-zero scalar, determine the same line. Expanding (A-6) yields,

$$\mathbf{S}_{0\mathbf{L}} = \begin{vmatrix} \mathbf{i} & \mathbf{j} & \mathbf{k} \\ x_1 & y_1 & z_1 \\ L & M & N \end{vmatrix} \tag{B-8}$$

Which can again be expressed as

$\mathbf{S_{0L}} = P\mathbf{i} + Q\mathbf{j} + R\mathbf{k}$ Where $P = y_1N - z_1M, Q = z_1L - x_1N, R = x_1M - y_1L$

Equation (B-5) becomes

$$LP + MQ + NR = 0 \tag{B-9}$$

Hence, $\{\mathbf{S}; \mathbf{S}_{0\mathbf{L}}\}$, the Plücker coordinates of the line becomes $\{L, M, N; P, Q, R\}$ [1]

APPENDIX C
VHDL CODE AND BLOCK DESIGN FILE USED ON THE FIELD PROGRAMMABLE GATE ARRAY FOR SIMULTANEOUS QUADRATURE DECODING OF THE SIX ENCODERS

C.1 Block Design File

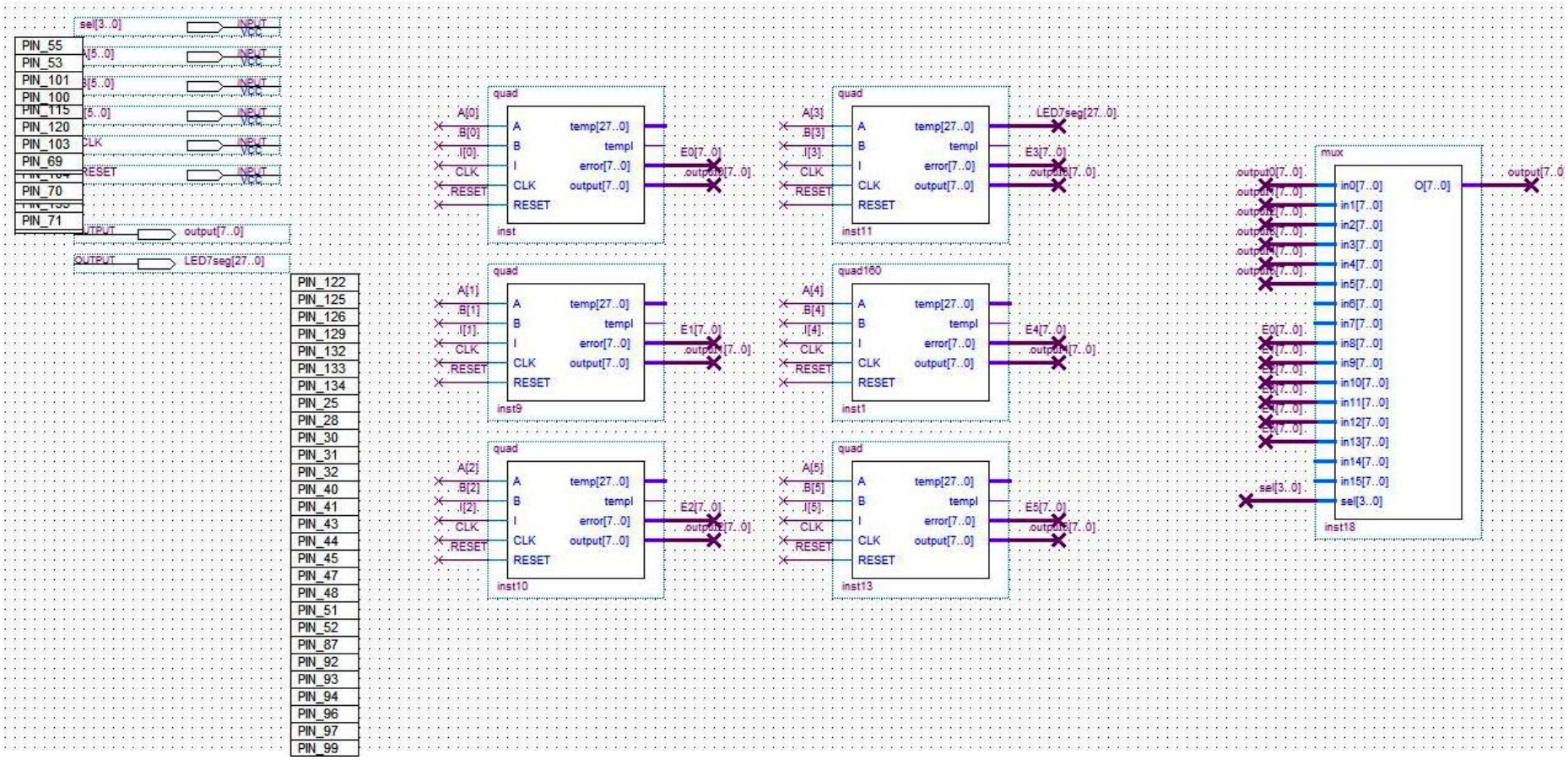

C.2 Quad.vhd

```
LIBRARY ieee;
USE ieee.std_logic_1164.ALL;
USE ieee.std_logic_arith.all;
USE ieee.std_logic_unsigned.all;
use ieee.numeric_std.all;

ENTITY quad IS
PORT(
                A, B, I : IN  std_logic;
                CLK, RESET : IN std_logic;
                temp : OUT std_logic_vector(27 downto 0);
                tempI : OUT std_logic;
                error : OUT std_logic_vector(7 downto 0);
                output : OUT std_logic_vector(7 downto 0)
);

END quad;

ARCHITECTURE logic OF quad IS

 signal R : std_logic_vector(7 downto 0);        -- Register holds current count
 signal TTTA, TTTB, TTA, TTB, TA, TB : std_logic;
 signal cntdir : std_logic;
 signal cnten : std_logic;
 signal S : std_logic;                          -- start bit, index controls
 signal diff : std_logic_vector(7 downto 0);

  COMPONENT decoder
   PORT(
        A               : IN     STD_LOGIC_VECTOR(3 DOWNTO 0);
        YN              : OUT   STD_LOGIC_VECTOR(6 DOWNTO 0)
       );
  END COMPONENT;

BEGIN
  PROCESS(CLK, RESET)
    BEGIN
      if(RESET = '0') then
         S <= '0';
         diff <= (OTHERS=>'0');

         R <= std_logic_vector(to_unsigned(100, R'length));
      elsif(CLK'event and CLK='1') then
```

```
                    if(I = '1') then
                            S <= '1';
                            tempI <= '1';
                       if(R = std_logic_vector(to_unsigned(100, R'length))) then
                         diff <= (OTHERS=>'0');
                       else
                         diff <= R(7 downto 0);
                         R <= std_logic_vector(to_unsigned(100, R'length));
                       end if;
                    else
                       tempI <= '0';
                    end if;

                    if(cnten = '1' and S = '1') then
                  if(cntdir = '1') then
                    R <= R + 1;
                  else
                    R <= R - 1;
                  end if;
                 end if;

            end if;
  END PROCESS;

  PROCESS(CLK)
    BEGIN
      if(CLK'event and CLK = '1') then
        TTTA <= A;
        TTA <= TTTA;
        TA <= TTA;

        TTTB <= B;
        TTB <= TTTB;
        TB <= TTB;
            end if;
  END PROCESS;

  cntdir <= TTA XOR TB;
  cnten  <= TTA XOR TA XOR TTB XOR TB;
  output <= R;
  error <= diff;
  LED0: decoder PORT MAP(R(3 downto 0), temp(6 downto 0));
  LED1: decoder PORT MAP(R(7 downto 4), temp(13 downto 7));
  LED2: decoder PORT MAP(diff(3 downto 0), temp(20 downto 14));
  LED3: decoder PORT MAP(diff(7 downto 4), temp(27 downto 21));
END logic;
```

C.3 Mux.vhd

```
LIBRARY ieee;
USE ieee.std_logic_1164.ALL;
ENTITY mux IS

PORT(
        in0, in1, in2, in3, in4, in5, in6, in7, in8, in9, in10, in11, in12, in13, in14,
in15 : IN STD_logic_vector(7 downto 0);
        sel : IN  STD_logic_vector(3 downto 0);
        O   : OUT STD_logic_vector(7 downto 0)
);

END mux;


ARCHITECTURE logic OF mux IS
BEGIN
    WITH sel SELECT
            O <= in0  WHEN "0000",
                 in1  WHEN "0001",
                 in2  WHEN "0010",
                 in3  WHEN "0011",
                 in4  WHEN "0100",
                 in5  WHEN "0101",
                 in6  WHEN "0110",
                 in7  WHEN "0111",
                 in8  WHEN "1000",
                 in9  WHEN "1001",
                 in10 WHEN "1010",
                 in11 WHEN "1011",
                 in12 WHEN "1100",
                 in13 WHEN "1101",
                 in14 WHEN "1110",
                 in15 WHEN "1111";
END logic;
```

APPENDIX D
MECHANICAL DRAWINGS OF THE PARALLEL MECHANISM

Refer to Bo Zhang’s Ph.D. Dissertation [12] for the same.

LIST OF REFERENCES

[1] Crane, C.D., Rico, J.M. and Duffy, J., 2001, EML6282 Geometry of Robots II Class notes: *Screw Theory and its Application to Spatial Robot Manipulators*, MAE, University of Florida, Gainesville, FL.

[2] Crane, C.D. and Duffy, J., 1998, *Kinematics Analysis of Robot Manipulators,* Cambridge University press, USA.

[3] Dwarakanath, T., and Crane, C. 2000, “In-parallel Passive Compliant Coupler for Robot Force Control,” *Proceedings of the ASME Mechanisms Conference*, Baltimore, MD, pp. 214-221.

[4] Duffy, J, 1996, *Statics and Kinematics with Applications to Robotics*, Cambridge University press, New York, USA.

[5] Future Technology Devices International Ltd., February 2006, Application Note – “AN232B-04 Data Throughput, Latency and Handshaking”, Glasgow, United Kingdom.

[6] Future Technology Devices International Ltd., January 2009, Software Application Development D2XX Programmer’s Guide – “API for the FTD2XX DLL function library”, Glasgow, United Kingdom.

[7] Griffis, M., and Duffy, J., 1989, “A Forward Displacement Analysis of a Class of Stewart Platforms,” Journal of Robotic Systems, Vol. 6(6), pp. 703-720.

[8] Griffis, M., 1991, “Kinestatic control: A Novel Theory for Simultaneously Regulating Force and Displacement”, Ph.D. Dissertation, University of Florida, Gainesville, FL

[9] Griffis, M., and Duffy, J., 1991, “Kinestatic Control: A Novel Theory for Simultaneously Regulating Force and Displacement,” Trans. ASME Journal of Mechanical Design, Vol. 113, No. 4, pp. 508-515.

[10] Lee, J., 1996, “An Investigation of A Quality Index for The Stability of In-Parallel Planar Platform Devices,” Master’s Thesis, University of Florida, Gainesville, FL.

[11] Quadrature Decoder [Internet] by Nicolle, Jean P. [updated 2008 Feb 13; cited 2009 Dec 04] Available from: http://www.fpga4fun.com/QuadratureDecoder.html

[12] Zhang, B., 2005, "Design and Implementation of a 6 DOF Parallel Manipulator with Passive Force Control," Ph.D. Dissertation, University of Florida, Gainesville, FL.

BIOGRAPHICAL SKETCH

Subrat Nayak was born in Rourkela, Orissa, India in 1983. He received his Bachelor of Technology degree in electrical engineering from National Institute of Technology, Rourkela, India in May 2005. He was also awarded the Best B. Tech Project Gold medal with his degree. He got excited about Robots during his undergraduate education and participated in numerous National Level Student Robotic competitions. He worked for two and half years at Satyam Computer Services Ltd, Chennai, India. Though joined as a Software Engineer, he got the opportunity to start a Robotics project and enjoyed coordinating the implementation of two Tour guide robots at the Satyam Automotive Centre of Excellence. During his time at Chennai, He also volunteered for AID INDIA, a non-profit organization in making inexpensive educational robots and scientific kits for unprivileged kids.

Passionate about working with robots and advance his education in robotics, he joined the Department of Electrical and Computer Engineering at University of Florida for a Master of Science degree. Since, then he has been working at Machine Intelligence Lab with Dr. Eric M. Schwartz. He has worked extensively on numerous Robots, namely the IMDL Robot, the Trash-collecting Robot for IEEE Hardware Competition, Human Powered Submarine for International Submarine Race and SubjuGator – Autonomous Submarine for AUVSI Underwater Vehicle Competition. He also worked as a Teaching Assistant for Electrical Energy Conversion Lab and Senior Design Lab at the Department of Electrical and Computer Engineering. He has been working on his Masters' Thesis with Dr. Carl D. Crane III at the Center for Intelligent Machines and Robotics. He is also enrolled for a second Master of Science degree in mechanical engineering.